Photophysical Properties and Excited State Dynamics of Porous Organic Materials

Korlan Duisenova
Marquette University

PHOTOPHYSICAL PROPERTIES AND EXCITED STATE DYNAMICS OF POROUS ORGANIC MATERIALS

by

Korlan Duisenova

A Thesis submitted to the Faculty of the Graduate School,

Marquette University,

in Partial Fulfillment of the Requirements for

the Degree of Master of Science

Milwaukee, Wisconsin

May 2020

ABSTRACT

PHOTOPHYSICAL PROPERTIES AND EXCITED STATE DYNAMICS OF POROUS ORGANIC MATERIALS

Korlan Duisenova

Marquette University, 2020

Charge transfer complexes are charge separated states that are formed at donor - acceptor interfaces and play significant role in charge photogeneration. One of the main criteria for efficient charge transfer is suppression of charge recombination process. Previous experiments show that one of the most effective ways to inhibit recombination is an introduction of bridge molecules between donor and acceptor or increase the number of electron donating and withdrawing groups. These solutions are inspired by photosynthetic reaction centers where charge transfer occurs over long distances. Covalent Organic Frameworks (COFs) are advanced porous crystalline materials that can be constructed of multiple donor and acceptor building blocks. This approach improves efficiency of charge transfer by suppressing dissociation of polaron pairs. In the present work, photophysical and charge dynamics processes of various donor-acceptor systems, namely star-shaped carbazole-π-triazine organic chromophores, BTPA-cased donor-acceptor COFs, and metallophthalocyanine COFs, were investigated using the combination of steady-state spectroscopic techniques and time-resolved femtosecond transient absorption (TA) spectroscopy.

The study on star-shaped carbazole-π-triazine organic chromophores showed that formation of charge transfer can be facilitated by positioning a bridging phenyl ring by creation of conjugated system. Nevertheless, the introduction of two phenyl bridge units can distort the coupling leading to weak charge migration from carbazole.

Combination of BTPA (5,5',5''-(1,3,5-Benzenetriyl)tris[2-pyridinecarboxaldehyde]) and a series of three different organic precursors: 1,3,5-Tris(4-aminophenyl)benzene (TPB), 4,4',4''-Triaminotriphenylamine (TPA), and 1,3,5-Tris(4-aminophenyl)triazine (TPT) for the synthesis of COF showed that efficient charge transfer and slower recombination process can be achieved by incorporating stronger electron donating group, such as TPA, to enhance excited state dipole moment.

Finally, the investigation of charge dynamics in COFs constructed using copper and nickel metallophthalocyanine linked to electron withdrawing 2,3,5,6-tetrafluoroterephthalonitrile (TFTPN) revealed the delocalization of charge between neighboring donor-acceptor units formed within 1.464 – 1.750 ps, which is further transferred between COF layers and dissociates between 0.662 – 3.383 ns.

Acknowledgements

First of all, I would like to express my gratitude and appreciation to Dr. Jier Huang for being excellent supervisor, mentor and teacher. Learning from Dr. Huang was a great enjoyable experience. Besides instructing me in Quantum Chemistry and Molecular Spectroscopy, Dr. Huang encouraged and guided me in my first steps to the research world. She spreads enthusiasm, positivity and will always serve me as a role model of successful scientist and chemist. I am also much grateful to my research committee members, Dr. Scott Reid and Dr. Qadir Timerghazin, for generously offering time and feedback on my seminar and the thesis.

I am very thankful to the members of the research group, James Nyakuchena, Dr. Sizhuo Yang, Wenhui Hu, Daniel Streater, Yixuan Zhou and Yunbo Yang. With the help of Sizhuo and Wenhui, I was able to learn the techniques and use of instruments necessary for the research I've done.

I would also like to offer special appreciation and respect to Dr. Vijay Vyas, who was my teaching supervisor, for giving me valuable feedback and supporting throughout four semesters of teaching. I was incredibly lucky to have Ainur Abzhanova, Fathiya Jahan and Niloufar Hendinejad, as my friends. The most wonderful moments at Marquette happened with you, girls.

I am eternally grateful to my beloved parents, Zharylgap and Nurgul, for their love, inspiration, motivation to study and always move forward. To my aunt Aigul, who inspired me to become a Chemist. Lastly, I would like to thank my fiancé and my best friend, Madi, for being my source of happiness, laughter and love; for constantly giving me moral support, and for just always being there for me.

TABLE OF CONTENT

LIST OF TABLES

LIST OF SCHEMES

LIST OF FIGURES

CHAPTER I: INTRODUCTION

1.1. Introduction to Charge Transfer between electron-rich and electron-poor units

The ever-rising energy consumption and the detrimental effect of the use of fossil fuels on the environment are serious global issues. According to the International Energy Agency report, in 2019 the global energy consumption increased by 2.3%. About 70% of this energy demand was fulfilled by the burning of fossil fuels. Fossil fuel combustion emitted 33.1 gigatons of carbon dioxide into the atmosphere along with carbon monoxide, nitrogen dioxide, hydrogen sulfide and other volatile organic compounds. The impact of such emissions on the environment is dramatic: greenhouse effect, increasing acidity of water, ozone layer depletion etc.

Finding alternate ways of generating energy is a challenge that calls for immediate attention. Thus, solar cells, wind turbines, hydrogen fuel cells, geothermal methods and other alternative energy sources are being sought after. One of the biggest shortcomings of the solar cells that are currently used is the high cost and the use of metals that limit the bulk production and use. Therefore, it is important to explore new materials that can be effective for this purpose. The investigation of these materials is often inspired by nature, where solar energy is efficiently harvested by plants using chlorophyll *a* and its auxiliary pigments, such as carotenoids. These pigments constitute an ‘antenna’ array, where irradiation of UV light causes a series of energy transfer (**EnT**) reactions (**Figure 1.1**).

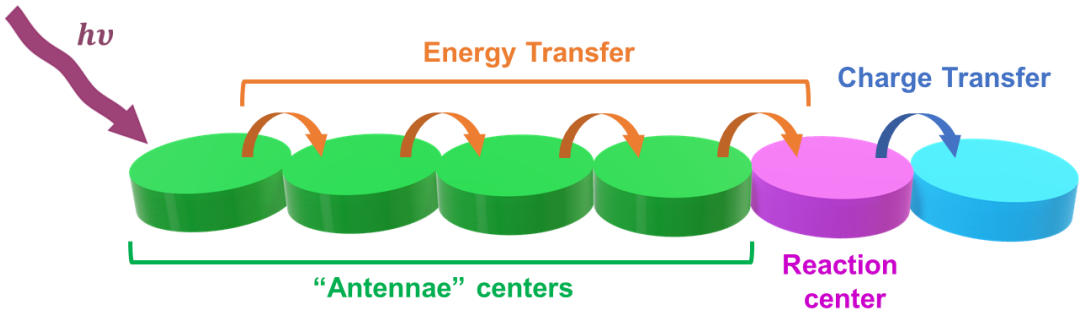

Figure 1.1. Photosynthesis mechanism involving EnT and charge transfer

An efficient light harvesting system is characterized by high absorption cross section (covering the UV and visible region), high charge carrier mobility and long-lived excited states. For example, chlorophyll largely absorbs light in the visible region of the electromagnetic spectrum. Upon photoexcitation, it relaxes back to the ground state and emits light, nearly 97% of which is absorbed by neighboring pigment in the 'antenna' centers. The chain reaction continues until the irradiated energy reaches reaction centers where electrons are transferred from water splitting in Photosystem II (**PSII**) to Photosystem I (**PSI**) resulting in the reduction of NADP to NADPH.[1–4] Photosynthesis is, therefore, a complex process that involves EnT and Charge Transfer (**CT**). Hence, developing an understanding of the electron transfer mechanism can help to mimic similar process for practical applications that can be scaled. Each elementary step in photosynthesis is a source of inspiration for designing materials that harvest solar energy for other applications, such as photocatalytic water splitting,[5,6] catalysis or capture CO_2 emissions.[7]

All light harvesting processes start with the formation to locally excited (**LE**) state (**Figure 1.2a**) formation followed by charge separation and transfer before recombination

can take place. Thus, CT is one of the key reactions that determine the efficiency of light harvesting.

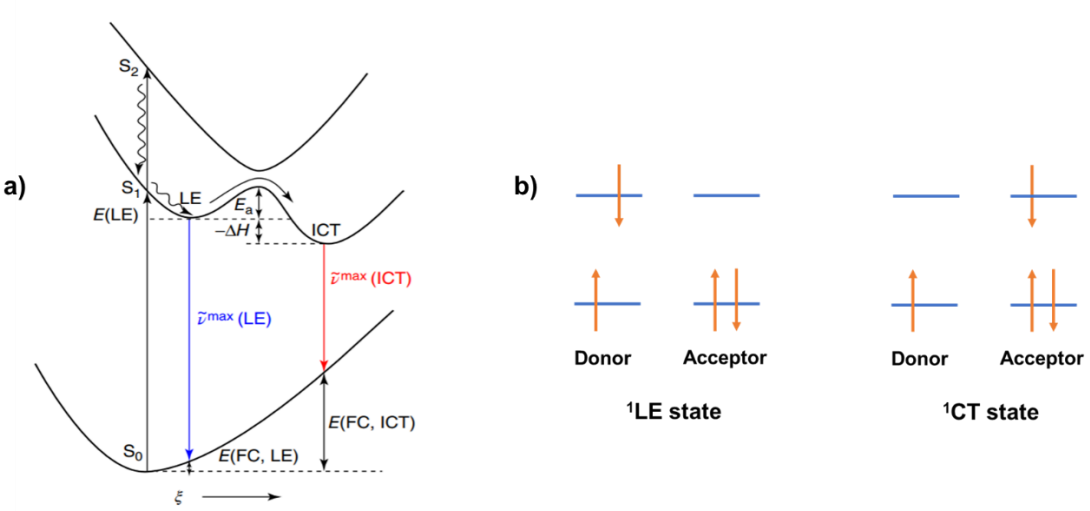

Figure 1.2. (a) Jablonski Diagram of ICT formation, (b) Electronic configuration of LE and CT state

Charge transfer refers to the transfer of electrons from an electron-rich (donor) to electron-poor part (acceptor) located within the same molecule (intramolecular CT, **ICT**) or between different molecules (intermolecular).[8] Thus, excitation of electron-rich part of molecule is the first step (**Figure 1.2b**). As shown in the Jablonski diagram (**Figure 1.2a)**, the charge separated state have a narrower band gap between highest occupied molecular orbital (**HOMO**) and lowest unoccupied molecular orbital (**LUMO**). This means that excitation to and relaxation from CT requires less energy as compared to the LE state, which may fall in the visible region of the electromagnetic radiation. This makes these molecules excellent candidates for visible light photocatalysis or visible light emitters. The oxidation of donor and the reduction of acceptor units result in the formation of electron-

hole pair, i.e. charge transfer process, which is a crucial step in solar energy conversion such as photocatalysis, photovoltaic devices and photoelectronics.

A fundamental understanding of the interaction between the D and A and the factors affecting this process is essential for further developing devices for solar energy conversion. A donor is a molecule or a part of a molecule which contains a free electron site, whereas an acceptor has a stronger electron affinity and attracts this electron. To explain the rate of CT in donor-acceptor systems, Rudolph A. Marcus developed a theory of electron transfer in 1956. According to Marcus's theory, ET rate (k_{ET}) follows Gaussian type dependence with respect to the Gibbs Free Energy of ET (ΔG_{ET})[9] and can be expressed in an Arrhenius-type equation:

$$k_{ET} = \sqrt{\frac{4\pi^3}{\hbar^2 \lambda k_B T}} H_{DA}^2 exp\left\{-\frac{(\Delta G_{ET}+\lambda}{4\lambda k_B T}\right\} \qquad (1)$$

where, k_B is a Boltzman constant and T is the absolute temperature at which charge transfer occurs.[10–13] Equation (1) shows that in order to achieve efficient CT, strong electron coupling between D and A (H_{DA}), solvent reorganization energy (λ) and ionization potential of D and electron affinity of A, which dictates ΔG_{ET}, must be controlled.

Gibbs Free Energy of Charge Transfer can be expressed according to Equation (2):

$$\Delta G_{ET}^{\circ} = e\left[E_{acceptor}^{\circ} - E_{donor}^{\circ}\right] - \frac{e^2}{4\pi\varepsilon_0\varepsilon_s d} \qquad (2)$$

where $E_{acceptor}^{\circ}$ and E_{donor}° are standard reduction and oxidation potentials respectively, ε_0 is vacuum permittivity, ε_s is dielectric constant of solvent and d the distance (d) between donor and acceptor.

H_{DA} can be rearranged in terms of the structure of the donor and acceptor. It decays exponentially as the distance (d) between donor and acceptor increases:

$$H_{DA} = Ae^{-\beta d} \qquad (3)$$

where β is pre-exponential factor called distance decay function. According to the work done by Oliver S. Wenger, β depends on the mechanism of CT.

CT follows two major paths: (a) hopping mechanism or (b) tunneling mechanism.[12,14,15] Wenger showed that when reduction of bridge units connecting donor and acceptor is thermodynamically favorable and the energies of donor and bridges are equivalent to each other, CT is activated through hopping or sequential mechanism (**Figure 1.3a**). In this case, the rate of CT is weakly related to distance (β is negligible).[12,16] CT dynamics strongly depends on the distance when tunneling or superexchange mechanism occurs (**Figure 1.3b**). Distance decay function (β) is significant and the reduction of bridge is thermodynamically unfavorable.[13,14,16]

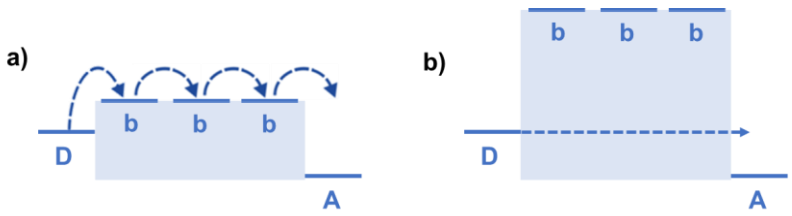

Figure 1.3. (a) Hopping mechanism, (b) tunneling mechanism

1.2. Experimental Techniques that Characterize Charge Transfer Process

Steady-state or linear electronic spectroscopy is one of the primary techniques to detect CT state. Electron coupling between a donor and acceptor, which leads to charge transfer under photoexcitation and sufficient redox potentials, narrows energy gap compared to

discrete excitation of donor or acceptor (**Figure 1.4a**). As a result, the absorption peak caused by CT appears bathochromic relative to LE states (**Figure 1.4b**). Electronically, the structure of CT state is composed of oppositely charged radical pairs of donor (D^+) and acceptor (A^-) (**Equation 4**):

$$\psi_{CT} = \psi_{D^+}\psi_{A^-} \qquad (4)$$

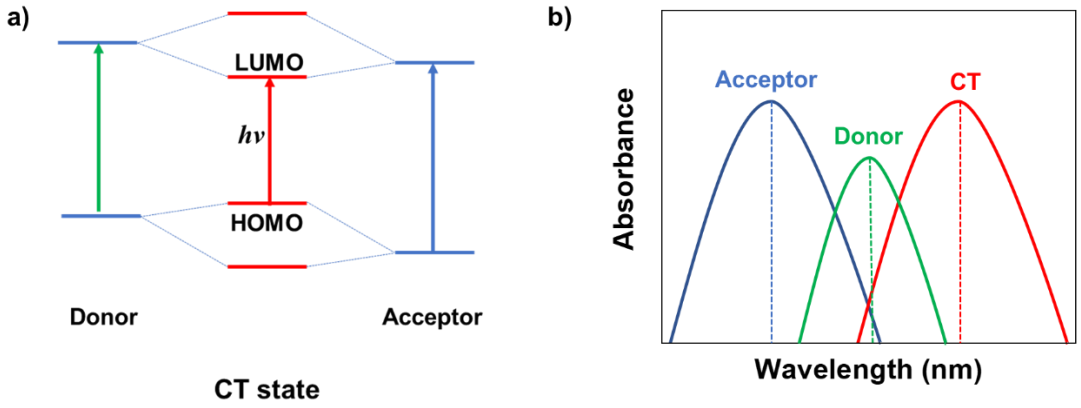

Figure 1.4. (a) Energy level representation of CT complex formation, (b) Example of steady-state absorption spectra showing red-shift in absorption due to CT

If the radiative relaxation of excitons to the ground state takes place from CT state, it is possible to locate it with the help of steady-state photoluminescence spectroscopy. As indicated, the electronic structure of CT complex is made of oppositely charged donor and acceptor radical pair with non-zero dipole moment. As a result, the stability of CT depends on the polarity of solvent (**Figure 1.5a**). In toluene, CT state is energetically less stable than LE state and therefore, the internal conversion of LE state to CT state is thermodynamically unfavorable. Hence, the excitons mostly relax from the LE state. When the molecules are dissolved in more polar solvent, such as THF, the potential energy of CT state gets lower and therefore, the energy barrier for internal conversion decreases allowing

transition from LE to CT state. The potential energy of CT state becomes lower than LE state as the polarity is further increased. This results in reduced band gap between ground and CT state in acetonitrile (ACN). As a result, the emission shifts towards longer wavelength with the increase in polarity of the solvent (**Figure 1.5b**).

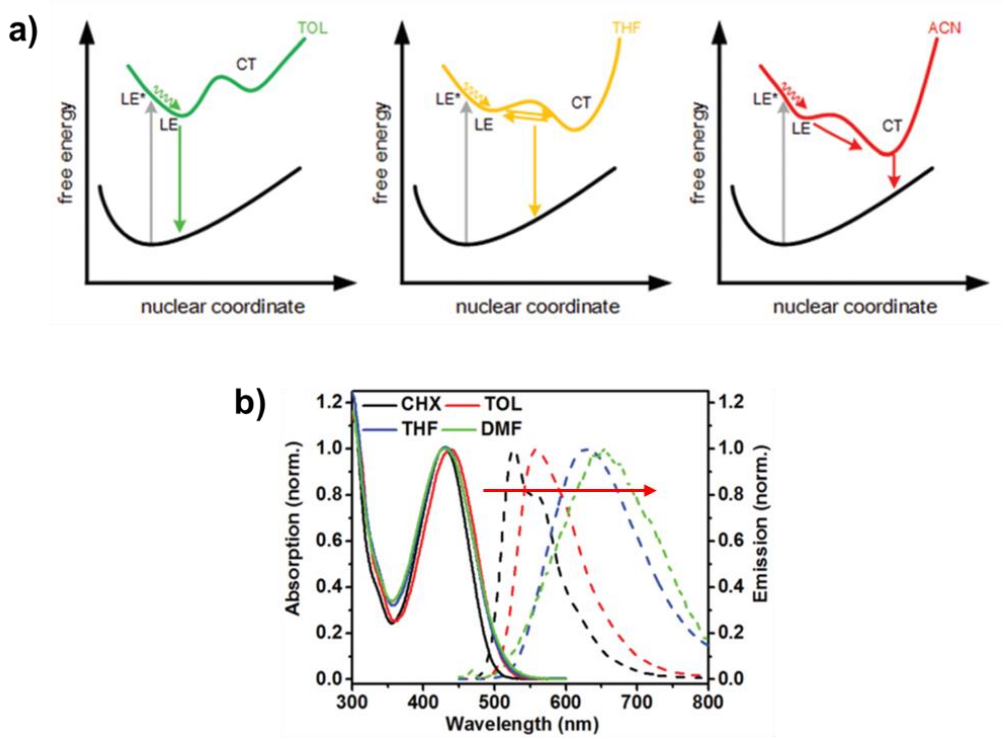

Figure 1.5. (a) Potential Energy Diagram of donor-acceptor system in solvents with different polarity (toluene, THF, acetonitrile), (b) steady-state absorbance and emission of donor-acceptor molecule in solvents with different polarity

While steady-state spectroscopy provides information on the energetics and relative dipole moment, ultrafast transient absorption (TA) Spectroscopy elucidates the dynamics of the excited state. The photophysical kinetics of the samples studied in this work is done by using TA spectroscopy, where molecules are promoted to the excited state using pump pulse at the required wavelength. This is followed by probe pulse with a delay time τ for probing the absorbance of molecules at excited state (A_{exc}). Measuring the absorbance in

the same manner without irradiation with pump laser ($A_{non\text{-}exc}$) results in the change in the population of the excited states within the delay time. TA spectroscopy measures these changes in the population by computing the difference in absorbances of the sample under irradiation of pump laser and the non-irradiated one:

$$\Delta A(\lambda, \tau) = A_{exc}(\lambda, \tau) - A_{non-exc}(\lambda, \tau) \qquad (5)$$

As the transient signal is the function of wavelength and time and it follows Beer - Lambert's Law. Equation (5) can be further expanded to:

$$\Delta A(\lambda, \tau) = \sum_i [\varepsilon_i(\lambda) - \varepsilon_0(\lambda)] c_i(\tau) \qquad (6)$$

Where, i is the number of excited state species, $\varepsilon_i(\lambda)$ is extinction coefficient of i^{th} excited state, $\varepsilon_0(\lambda)$ is molar extinction coefficient of the ground state species and $c_i(\tau)$ is the population of excitons after delay time τ. Therefore, using kinetic traces generated from transient signals, it is possible to derive extinction coefficients of excitons, the time constants associated with the transitions, and decay of these species. This provides information on the photophysical excited state transformation of the sample.

1.3. Construction of donor-acceptor systems

Donor-acceptor junctions are important in natural processes, like photosynthesis and respiration, as well as in photocatalysis and charge transfer photovoltaics devices such as OLEDs and solar cells.

Identification of molecules that carry potential to work as important candidates for efficient CT is the key to design such systems. **Figure 1.6** provides the structure of some of the commonly used donor and acceptor molecules employed in CT studies.[17]

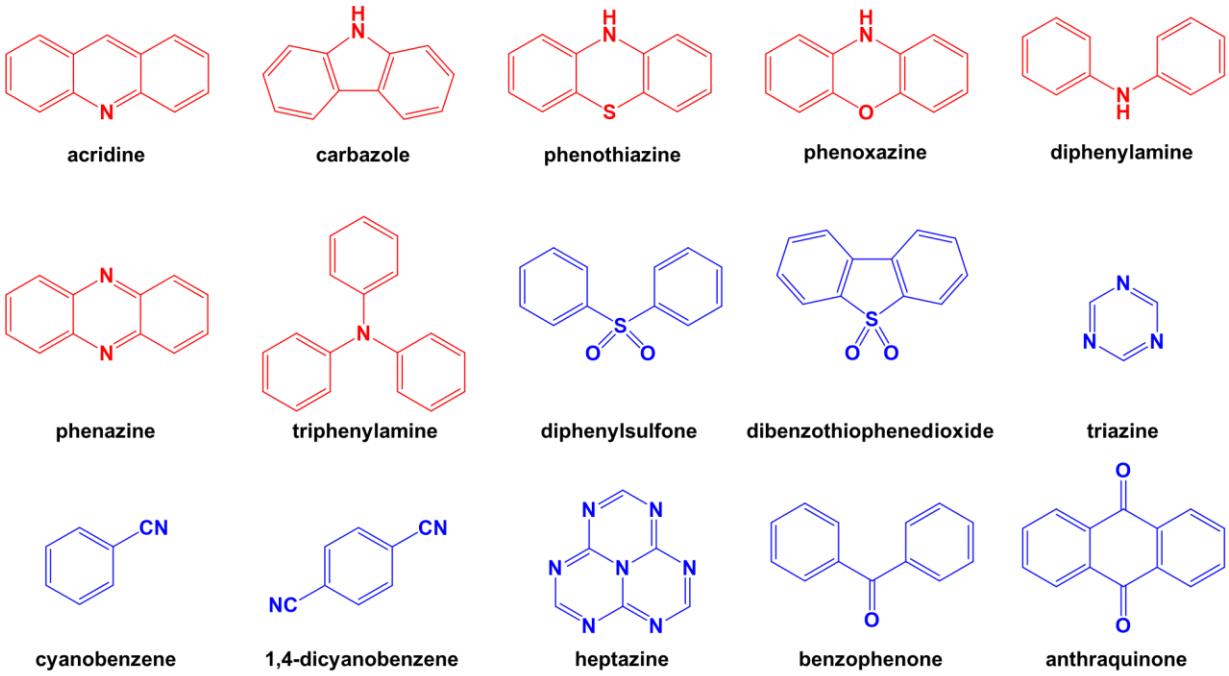

Figure 1.6. Structures of donor (red) and acceptor (blue) molecules[17]

The efficiency of CT is determined by the ability of the system to impede backward charge recombination. Learning from the structure of PSII in chloroplasts, this can be achieved by constructing CT systems that are separated by a long-distance. For example, Park et al. in 2012 investigated the effect of phenothiazine spacer group (PTZ) between donor and acceptor on charge recombination time constant of organic dyes in dye-sensitized solar cells. Figure 7 provides time constants for three DA systems as a function of photocurrent density where the synthesized dyes were coated on TiO_2 film. As can be seen in **Figure 1.7b**, the charge transfer rate is relatively similar for D-PTZ-A, D-PTZ1-PTZ2-A and conventional ruthenium based N719. However, charge recombination process for donor-acceptor system with two phenothiazine spacer groups is slower and the time constant follows the following trend:

$$\tau_{CR}(\text{D-PTZ1-PTZ2-A}) > \tau_{CR}(\text{D-PTZ-A}) > \tau_{CR}\ (\text{N719}).$$

The delay in charge recombination with an increase in the number of spacer molecules can be explained by the increased distance, the bent structure and steric hindrance, which is induced by the introduction of PTZ group between donor and acceptor.[18]

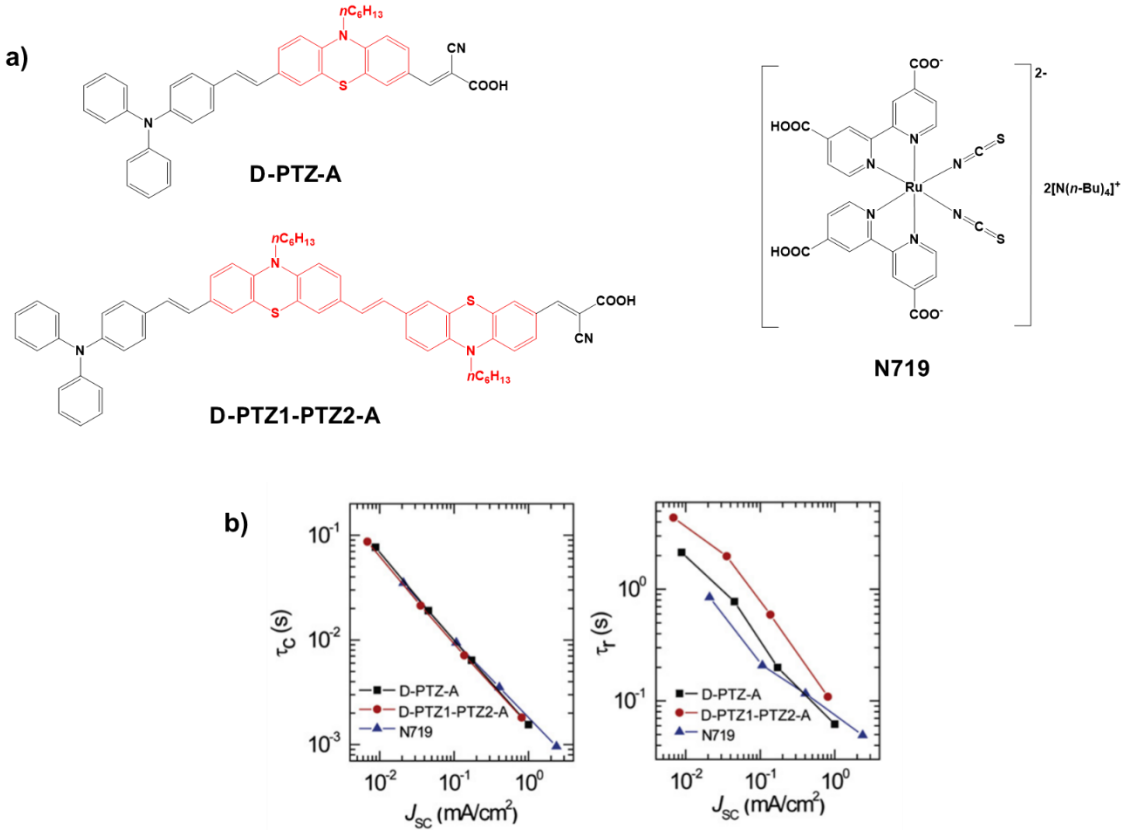

Figure 1.7. (a) structure of D-PTZ-A, D-PTZ1-PTZ2-A, and N719, (b) time constants for charge transfer (left) and charge recombination (right) as a function of short-circuit photocurrent[18]

Another way to inhibit charge recombination is to construct CT systems with multiple donor and acceptor units. This can be rationalized by the increased number of accessible energy levels introduced by the presence of multiple electron-rich and poor units that allow an efficient charge separation before recombination can take place (**Figure 1.8**). It is also associated with the migration of electron over longer distances as well.

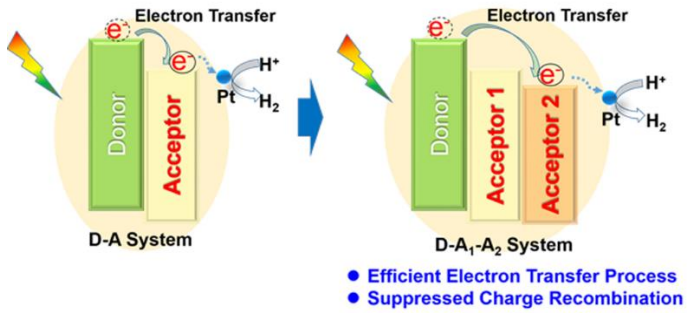

Figure 1.8. CT process *in donor-accept*or and *donor-acceptor 1-acceptor 2* system

Based on the features used to increase the efficiency of CT, donor-acceptor systems can be constructed either by synthesizing small molecular systems or polymers. In both cases, the electron donating and withdrawing units can be separated through π-bridge extending the conjugation of orbitals promoting delocalization of electron. The advantages of designing small molecules include the purity of material and their ability to crystalize into long-range order.[19] However, the CT in molecular systems is restricted within small distance, as they tend to form non-homogeneous aggregations.[19] On the other hand, polymeric conjugated systems show a tendency to arrange themselves in stacked position.[20–23] As a result, upon ordered and periodic arrangement of 2D layers, π-conjugation throughout 3D network is formed as well. This allows delocalization of electrons along conjugated backbone and π-stacking resulting in migration of charge across longer distances and a lower recombination rate.[23,24] Moreover, polymers can be prepared in bulk as compared to molecular systems where synthesis cannot easily be scaled.[25] The drawbacks of polymeric donor-acceptor systems include less defined structure of the polymer and in solubility in most solvents.[19,25]

1.4.Covalent Organic Frameworks

Covalent Organic Frameworks (COFs) are a class of porous organic macromolecules constructed from organic building blocks that contain light elements (C, H, N, O, B, etc.) that are connected through strong covalent bonds.[22,26,27] COFs are characterized by long-range ordered structure and crystallinity. The first COF was synthesized by Yaghi *et.al.* in 2005 through condensation reaction between phenyl diboronic acid $C_6H_4[B(OH)_2]_2$ and hexahydroxytriphenylene $[C_{18}H_6(OH)_6]$.[28] Since then, COFs are extensively investigated as photocatalysts,[29–33] semiconductors,[34–37] luminescent sensors;[27, 38–41] materials for energy storage,[42–45] proton conduction,[46–49] adsorption[50–55] and gas separation,[56] antibacterial activity[57] and drug delivery.[58]

The reversible covalent bond formation in COFs allows periodic and ordered arrangement of the building blocks resulting in overall long-range crystallinity of COFs. Moreover, reversible bond formation of COFs allows control of chain growth, tunable morphology and structural diversity. The building units used in COF formation usually contain multiple reactive sites. A certain geometry is required for polygon 2D structure and extension of network.[59,60] As can be seen in **Figure 1.9a**, it is possible to design well-defined 2D COF by following geometry matching of precursor units located at knots and as linkers.[59] Correspondingly, incorporation of tetrahedral-shaped or cross-linked building blocks results in the formation of 3D COFs (**Figure 1.9b**).[22] The additional characteristics of these materials include light weight, low density, large surface area, and prolific porosity.[22,26,61,62]

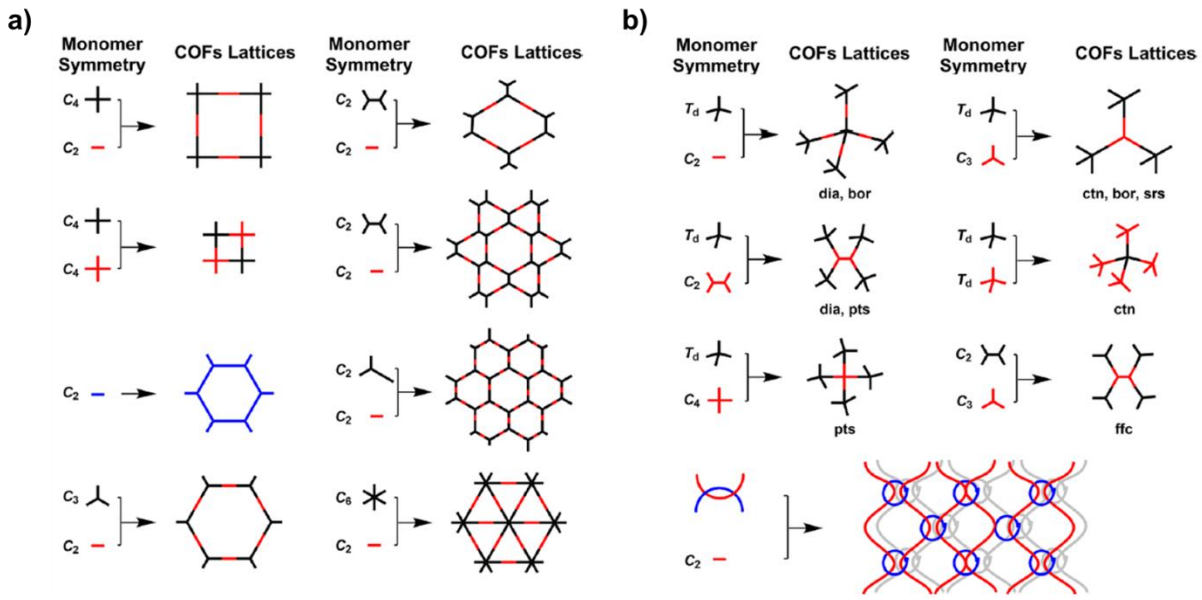

Figure 1.9. Structural diagrams of (a) 2D and (b) 3D COFs

Jiang *et.al*. synthesized a variety of COFs containing donor-acceptor systems. In one of these studies, they synthesized COF with multicomponent donor-acceptor system latticed into π-array, where 2,3,6,7,10,11-triphenylenehexol (**TP**) and bis(pinacol ester) (**E3**) are incorporated as electron-donating groups, whereas benzo[c][1,2,5]thiadiazole-4,7-diyldiboronic acid (E_2) is used as electron-accepting group (**Figure 1.10a**). The charge transferring ability of COF was analyzed using UV-visible absorbance spectra (**Figure 1.10b**), which show near-IR CT band peaking at ~800 nm. Moreover, the current-voltage characteristics of this COF demonstrates 180% increased conductivity compared to other COF samples described in this work (**Figure 1.10c**, red line).[59] Therefore, formation of COF containing multiple donor and acceptor precursor units can lead to increased electron mobility resulting in conductivity, offer enhanced structural diversity and complexity.

Another example of a donor-acceptor COF was published in 2015 for a COF formed by the polycondensation reaction between nickel, copper, zinc metallophthalocyanines (donor) and diimides (acceptor).[63] The results of X-ray diffraction pattern demonstrated well-defined structure consisting of donor-acceptor heterojunctions stacked in donor-to-donor and acceptor-to-acceptor manner (**Figure 1.11**). More specifically metallophthalocyanine and diimide units are covalently linked through boronate ester bonds extending its structure to tetragonal polygon. The high-order structure of the given COFs involves crystallization of tetragonal planes resulting in π-columnar arrays.[63]

The steady-state absorbance spectra of (D_{CuPc}-A_{PyrDI}-COF, **Figure 1.12a**) showed Soret band between 250 – 448 nm, corresponding to excitation from ground state (S_0) to second singlet excited state (S_2) (**Figure 1.12b**). The Q band ($S_0 \rightarrow S_1$ excitation) appears at around 687 nm. The absorption profile resemble absorption spectrum of copper phthalocyanine with a blue-shift of 30 nm in Soret band and 9 nm red-shift in Q band. The absence of other peaks in near IR (> 1500 cm^{-1}) region shows no indication of CT process between neighboring phthalocyanine and diimide group located in the same plane. However, TA spectrum shows the possibility of photoinduced CT when the metallophtalocyanine unit is excited. The results demonstrate that when the donor is excited, electron can migrate to four proximate and eight remote acceptor units in the framework (Figure 11a). The possibility of CT to a distant building block has a very low probability. Moreover, charge separated state resulting in oxidized donor radical and reduced acceptor radical can trigger electron-hole delocalization along the π-columns either in the same or opposite directions. The migration of electron into opposite directions leads to long-lived charge separation. It was found that the time constant for photoinduced

CT and formation of CS state is 1.6 ps, whereas the lifetime of this CS is 33 μs (**Figure 1.12c**).[63] Such slow charge recombination process can be very useful for its further application such as photoenergy conversion and OLEDs.[23,24,64]

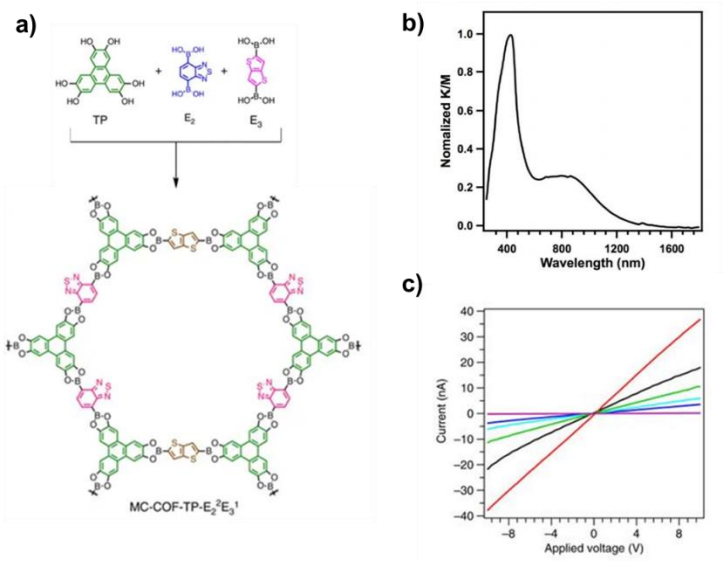

Figure 1.10. (a) structure of MC-COF-TP-E_2^2-E_3, TP, E_3 (donors), and E_2 (acceptor), (b) UV-visible absorbance spectrum of MC-COF-TP-E_2^2-E_3, (c) I-V curve of multiple component COF samples (MC-COF-TP-E_2^2-E_3 is given as red line)

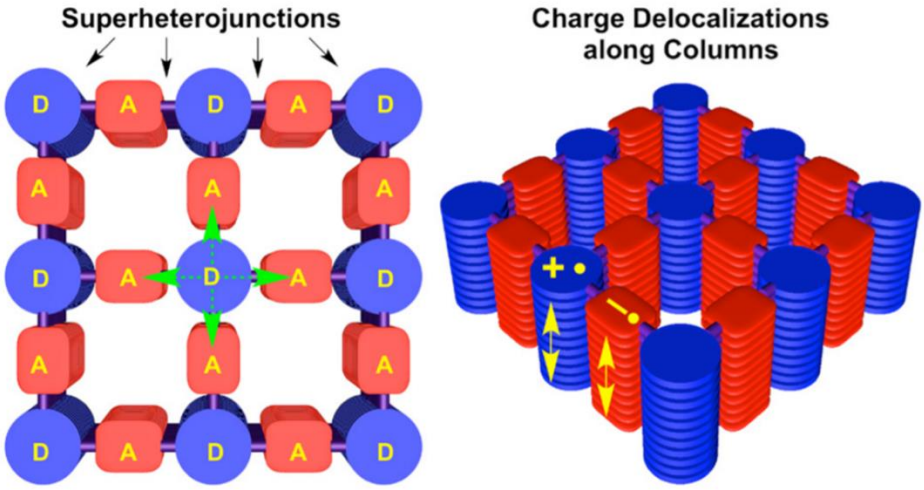

Figure 1.11. Schematic representation of periodic arrangement of donor-acceptor in metallophthalocyanine-diimide COFs

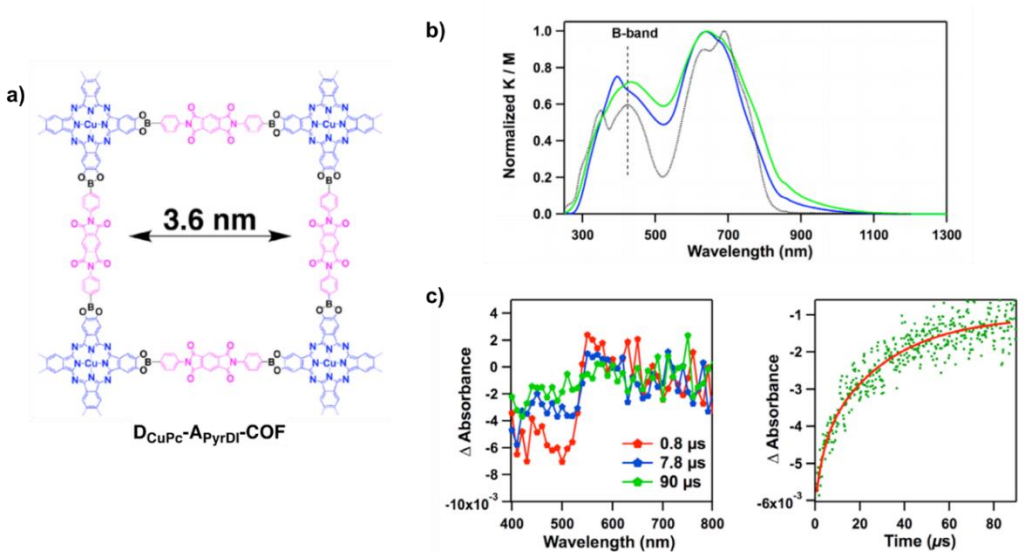

Figure 1.12. (a) Structure of D_{CuPc}-A_{PyrDI}-COF, (b)UV-visible absorbance spectra of D_{CuPc}-A_{PyrDI}-COF (green line) and CuPc[OMe]$_8$ (dotted line), and (c) TA spectra at 355 nm laser excitation and decay profile of D_{CuPc}-A_{PyrDI}-COF

1.5.Summary of the Research

These examples show that incorporation of donor-acceptor units into periodically arranged crystalline structures can help to develop new class of organic semiconductors. The advantages of such materials include affordability, wide optical range, structural diversity and flexibility. The investigation of photophysical processes plays important role in qualitative design of COF materials and other organic molecular systems that are able to generate long-lived charge separated state and be used in photovoltaics. The purpose of this work is to explore the excited state processes taking place in multiple donor containing star-shaped molecular systems and donor-acceptor COFs.

In the second chapter of this work, a series of triazine-phenylene-carbazole star-shaped donor-bridge-acceptor (D-B-A) molecules with 0, 1 and 2 bridging phenylene units are studied by steady-state spectral methods and TA spectroscopy. The bridge length is

varied to introduce structural and electronic differences across the series and impact on charge carrier dynamics is observed. The positioning of the three donor branches all meta- to one another also played a large role in the charge transfer process by directing electron donation to a specific site on the acceptor triazine unit. The spectroscopic data suggests that the distance between donor and acceptor, electron coupling between them and phenylene rings can significantly affect CT processes.

Further the photophysical properties of three COF samples synthesized through condensation reaction between BTPA (5,5',5''-(1,3,5-Benzenetriyl)tris[2-pyridinecarboxaldehyde]) with three different precursors: 1,3,5-Tris(4-aminophenyl)benzene (**TPB**), 4,4',4''-Triaminotriphenylamine (**TPA**), and 1,3,5-Tris(4-aminophenyl)triazine (**TPT**). The solid state absorption analysis shows bathochromic shift of COF samples compared to the building block molecules. The delamination of COF layers in ethanol contributed to better solubility and more resolved UV-visible steady-state absorption results. Moreover, we were able to achieve photoluminescence data of exfoliated COF samples in ethanol, which indicated analogous emission wavelength compared to counter-BTPA units (TPB, TPA and TPT). TA profiles revealed CT processes for three COF samples.

In Chapter IV the charge dynamics of donor-acceptor COFs constructed using copper and nickel phthalocyanine as electron-donor and 2,3,5,6 - tetrafluoroterephthalonitrile as electron-acceptor were investigated. The TA spectra shows the formation CT complex between neighboring donor-acceptor units as well as electron migration processes between COF layers due to their π-interactions. The ability of COFs to delocalize electron through π-columnar arrays suppresses rapid charge

recombination and therefore, this property of metallophthalocyanine COFs can find practical use in photoltaics and optoelectronics.

CHAPTER II: THE IMPACT OF π-CONJUGATION LENGTH ON EXCITED STATE DYNAMICS OF STAR-SHAPED CARBAZOLE-II-TRIAZINE ORGANIC CHROMOPHORES

2.1 Introduction.

Conjugated donor-bridge-acceptor (D-B-A) organic molecules have attracted increasing research attention owing to their potential application in photocatalysis[65,66], photovoltaics[67,68], organic light-emitting diodes (OLEDs)[69,70], and thin-film transistors[71]. A particular interesting class of these D-B-A organic molecules are those possessing star-shaped structure, which typically consist of an aromatic, heteroaromatic or triphenyl core to which electron-donating groups are radially attached as arms or arms containing electron-accepting units are attached to electron-donating core[72–74]. Due to these unique structures, star-shaped D-B-A organic molecules often display photophysical properties that are distinct from their linear analogues including improved processability in solution, facilitated electrical transport property, as well as the capability to organize into a supramolecular assembly.[75–77]

It has been shown that the key property that dictates the function of D-B-A star-shaped molecules in photocatalysis[78] and optoelectronics[79,80] is the intramolecular charge transfer (ICT) states. Previous studies demonstrated that the structural characteristics in donor-acceptor (D-A) and D-B-A molecules play an important role in the mechanism of ICT, such as π-conjugated linker distance[81,82], and the torsion between donor, bridge and acceptor[83,84]. For example, it has been found that the electron transfer mechanism through the bridge plays an important role on charge carrier kinetics of ICT.[10,12] If the electron travels through the virtual state of the bridge, which is energetically higher than the highest occupied molecular orbital (HOMO) of the donor, the ICT rate is sensitive to the distance

of the bridge. In contrast, when the HOMO of the linker is energetically close to or lower than the HOMO of the donor, the mechanism of ICT was believed to be "electron hopping" from donor to acceptor. Torsional angles between electron transferring groups is another factor that determines the pathway of ICT. Studies have shown that a perpendicular configurations of donor and acceptor orbitals can facilitate spin-flip upon electron transfer due to significant change in orbital angular momentum[85] when light absorption involves reverse intersystem crossing (RISC). Other studies have shown that planar conformations in ICT compounds can promote charge carrier mobility.[86]

As these studies strongly demonstrate the importance of the structure of D-B-A molecules to ICT, it is essential to develop a fundamental understanding of the correlation of the structure of the D-B-A star-shaped molecules with their ICT properties. In this work, we report a systematic photophysical study on a series of D-B-A star-shaped organic molecules using 2,4,6-triphenyl-1,3,5-triazine core as the electron-withdrawing acceptor and 3,6-di-*tert*-butyl-9-phenyl-9*H*-carbazole as the electron-donating arm which are connected via a series of 0, 1 and 2 phenyl rings as bridge (**Scheme 2.1**). Using the combination of steady-state and time-resolved absorption spectroscopy, we show that tuning the distance between D and A in D-B-A molecules via the number of phenylene ring bridge can dramatically impact the degree of ICT characteristics and the extent of conjugation. The spectroscopic results were supported by theory, where the results from time dependent density functional theory (TD-DFT) calculation suggest that ICT through conjugated π-orbitals, ground state torsional angles, and conformational relaxation from excited state are regulated by the presence of phenylene bridges between D and A.

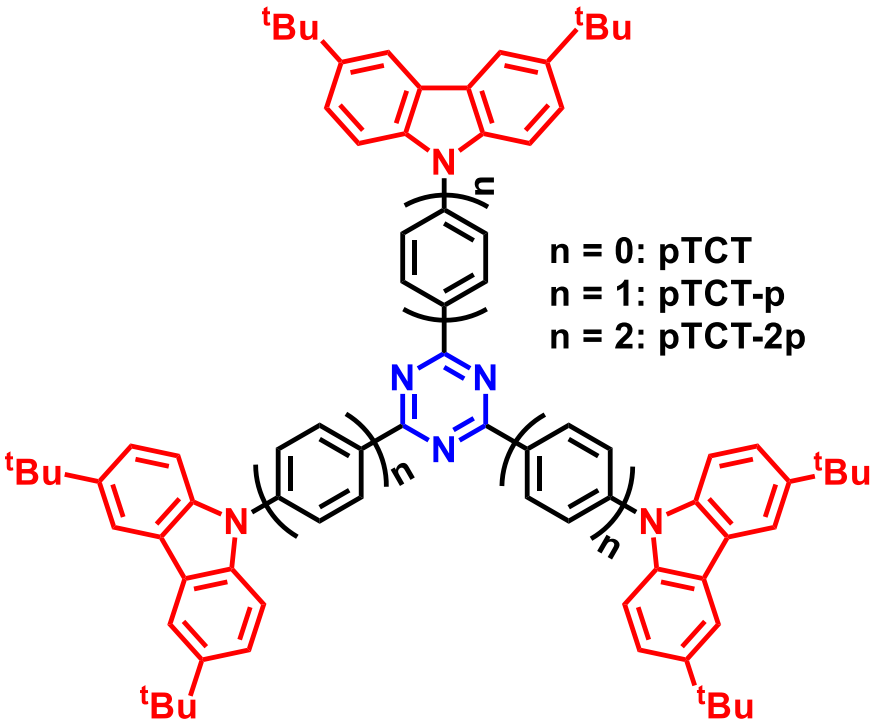

Scheme 2.1. Chemical structure of TCT series molecules

2.2. Experimental.

Standard Characterization. For steady-state absorption and luminescence measurements, 500 μM 2,4,6-triphenyl-1,3,5-triazine (acceptor), pTCT, pTCT-P, pTCT-2P and 1500 μM solution of 3,6-di-*tert*-butyl-9-phenyl-9*H*-carbazole (donor) in toluene were used. Samples were placed in 10 mm quartz cuvettes (Starna). UV-visible absorption measurements were carried out using Agilent Cary 300 UV-vis spectrometer. Steady state luminescence data were obtained on a PTI QM40 Spectrophotometer implemented with 75 W Xenon Lamp as excitation source and controlled by Felix GX Software. The emission lifetime of pTCT, pTCT-P, and pTCT-2P (100 μM) in toluene were collected using PTI TCSPC Spectrometer Felix GX Software at given emission wavelength. The solutions

were purged with N_2 for 15 minutes in 10 mm quartz cuvettes (Starna) before each measurement.

Transient Absorption Spectroscopy. Femtosecond Transient Absorption experiments were performed on a Helios Spectrometer (Ultrafast Systems LLC). The pump and probe pulses were generated using Ti-Sapphire laser system (Solstice, 800nm, 3.5 mJ/pulse, 1 KHz repetition rate). Pump is delivered from TOPAS using 75% yield of Ti:Sapphire laser chopped at 500 Hz. The generation of white light continuum (probe) takes place using 25% output of the amplifier and sapphire crystal.

500 μM solutions of 2,4,6-triphenyl-1,3,5-triazine, pTCT, pTCT-P, pTCT-2P and 1500 μM solution of 3,6-di-*tert*-butyl-9-phenyl-9*H*-carbazole in toluene were transferred into 2 mm quartz cuvette with a septum and purged in N_2 atmosphere. A PTFE-coated stir bar allowed continuous stirring during the measurements. pTCT, pTCT-P, pTCT-2P and donor samples were measured at 340 nm pump pulse with 0.3 mW power, while 300 nm pump pulse with 0.3 mW power was used for acceptor solution.

2.3. Results and Discussion

Figure 2.1 shows the steady state absorption spectra of pTCT, pTCT-P, and pTCT-2P, as well as 1,3,5-triphenyltriazine (acceptor) and 3,6-bis(*tert*-butyl)carbazole (donor). A common absorption peak at ~280 nm was observed for pTCT, pTCT-P and pTCT-2P (**Figure 2.1a-2.1c)**. This peak is also observed in the spectrum of the acceptor (**Figure 2.1d**) and donor (**Figure 2.1e**) and thus can be assigned to the local excitation (LE) band of either/both of these moieties. Compared to the spectra of donor and acceptor, an additional band was observed at 340 nm (pTCT), 395 nm (pTCT-P), and 370 nm (pTCT-

2P), which can be attributed to the intramolecular charge transfer (ICT) from carbazole donor to triazine acceptor. The ICT band is more blue-shifted for pTCT (340 nm) and red-shifted for pTCT-P (395 nm), which can be explained by extended conjugation due to phenylene bridge between donor and acceptor in pTCT-P.[87] The absorption peak of pTCT-2P appears at lower wavelength (370 nm) compared to that of pTCT-P although the donor and acceptor in pTCT-2P are connected through two phenylene rings, which may result from the disrupted conjugation by non-planar orientation of the bridge molecules to each other and is further supported by our computational results discussed later. Moreover, it should be noted that the absorption intensity of ICT band is comparable with LE band in pTCT and pTCT-P, whereas the intensity of ICT in pTCT-2P is significantly decreased at

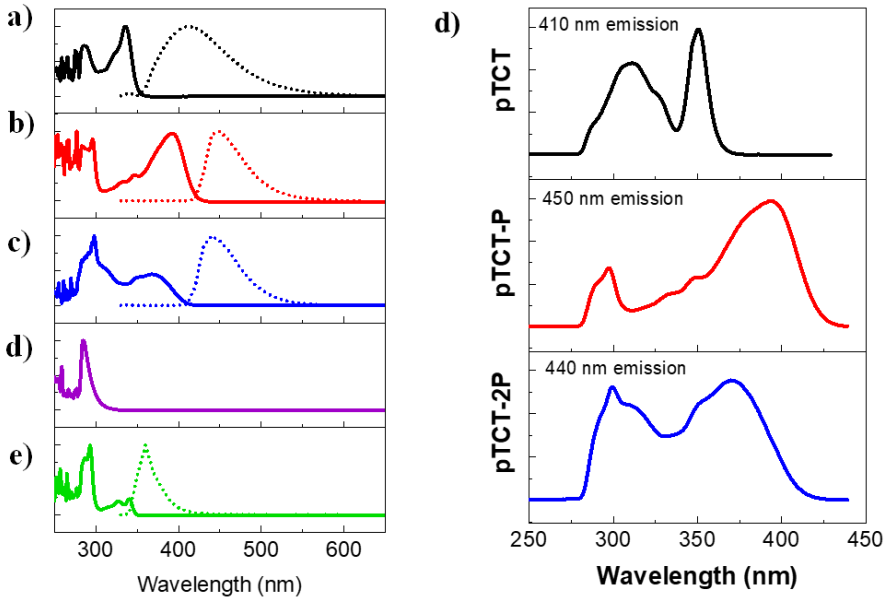

Figure 2.1. Normalized absorption spectra (solid lines) and steady-state emission spectra (dotted lines, 340 nm excitation) of a) pTCT, b) pTCT-P, c) pTCT-2P, d) acceptor, and e) donor and (f) Excitation spectrum of pTCT series molecules at indicated emission

370 nm compared to LE peak. This can be attributed to that the increased distance between donor and acceptor may obstruct the charge transfer process.

The emission spectra of these molecules are also presented in **Figure 2.1a-2.1c** (dotted lines). Similar to their absorption spectra, the emission wavelength increases from pTCT to pTCT-P and then blue-shifts slightly in pTCT-2P under excitation at both 280 and 340 nm. Because the emissions from pTCT, pTCT-P and pTCT-2P show red-shift with respect to that of donor suggesting that emissions of these three samples come from ICT state rather that LE state. The excitation spectra provide further evidence for the origin of emission in pTCT series. As shown in **Figure 2.1d,** the predominant emission at 450 nm in pTCT-P occurs from the 395 nm ICT state rather than the 300 nm LE state. The similar results were observed in pTCT, where the ICT state contribute more to the 410 nm emission than the LE state.

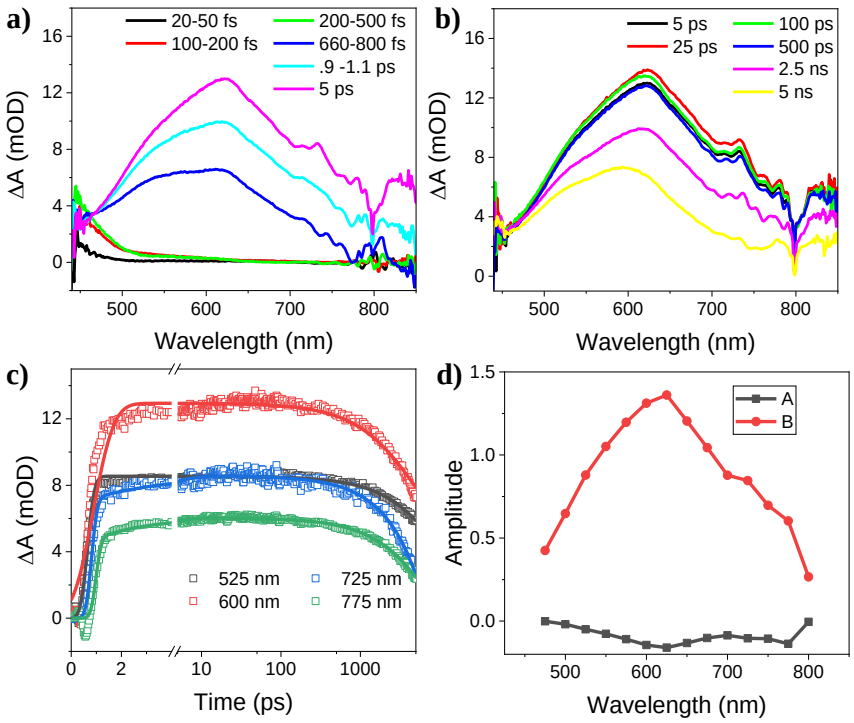

Figure 2.2 Kinetic decay profiles of (a) TPB-COF, (b) TPT-COF, (c) TPA-COF**.** (a) and (b) Femtosecond TA-spectrum of 3,6-bis(*tert*-butyl)carbazole at 340 nm excitation. (c) Fitted Kinetic Traces of TA spectra at given wavelength; (d) Species-associated difference spectra derived from Global Fitting Analysis

In order to gain further insight on the impact of bridge distance on the photophysical properties of pTCT, pTCT-P and pTCT-2P, we compared the excited state (ES) dynamics of these molecules using transient absorption (TA) spectroscopy. The TA spectra of acceptor and donor were also collected and used as control to account for the ES dynamics upon local excitation of these molecules (**Figure 2.2** and **2.3**). As shown in **Figure 2.3,** immediately following the excitation at 340 nm, a broad absorption feature centered at 625 nm is observed in the TA spectra of donor molecules. This feature gradually grows at 25 ps and then decays until 5 ns, which reaches the limit of our TA time window.

More complicated spectral evolution was observed in the spectra of acceptor. As shown in **Figure 2.3,** three main regions can be highlighted in the TA spectra of the acceptor. At very early time (<500 fs), we observed the formation of an absorption peak at 475 nm, which quickly decays and evolves (~5 ps) to form an absorption feature with double-lumps at 600 and 650 nm. The double-lump absorption feature then decays, which is accompanied by the formation of a peak at 525 nm. The 525 nm peak is super-long lived as negligible decay was observed within the 5 ns time window of the TA spectroscopy. The computational calculations suggest that the double-lump absorption peaks appearing at 600 and 650 nm correspond to charge transfer (CT) from phenyl rings to triazine center. Therefore, excitation of acceptor molecule at 300 nm first generates locally excited (LE) state at 475 nm at phenyl moiety, which then rapidly donates charge to triazine part undergoing intersystem crossing (ISC) to CT state (600 and 650 nm). Multiple small-

energy absorption features at >700 nm can be assigned to Frack-Condon relaxation in the excited state of triazine center.

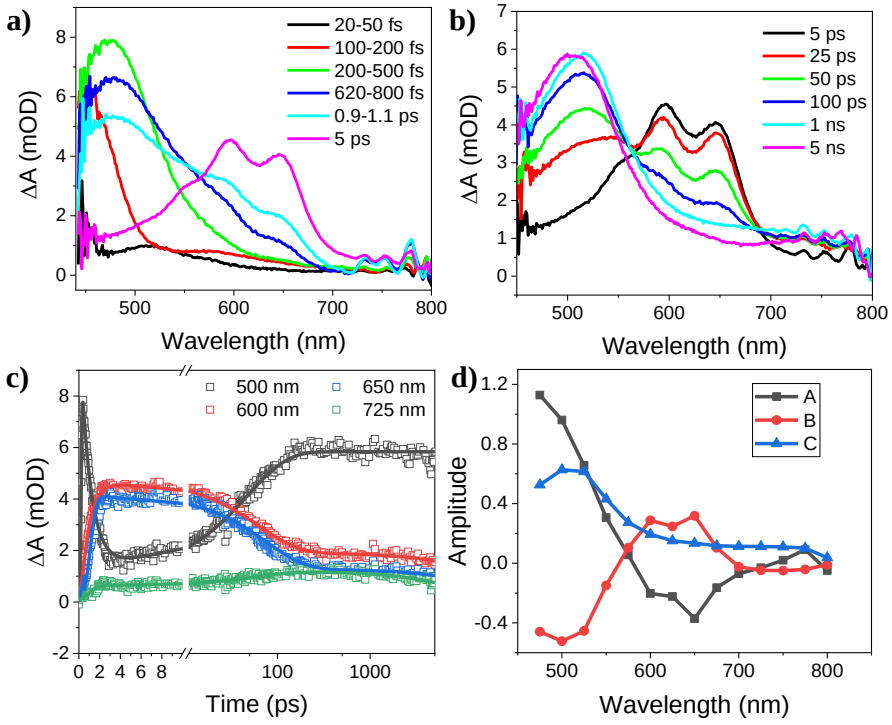

Figure 2.3. (a) and (b) Femtosecond TA-spectrum of 1,3,5-triazine (acceptor) at 300 nm excitation. (c) Fitted Kinetic Traces of TA spectra at given wavelength; (d) Species-associated difference spectra derived from Global Fitting Analysis

In the TA spectra of pTCT, we observed rapid rising of broad band centered at 550 nm following 340 nm excitation at early time (<1 ps, **Figure 2.4a**). After that (~1 ps-5ps), this band decays and evolves to form another absorption band centered at 725 nm, 750 and 775 nm, which decays afterwards (**Figure 2.4b**). These triple ESA peaks at > 700 nm were also observed in the TA spectra of acceptor, suggesting that this feature is a CT state from the donor to the acceptor (**Figure 2.3**). On the other hand, the broad peak centered at ~525 nm is observed neither in the TA of donor nor acceptor. However, slowly decaying 525 nm absorption has a shoulder around ~625 nm that is prominent in the TA spectrum of

donor, suggesting that the exciton has more characteristics of a donor localized hole. Additionally, it can be reasoned that transient spectral shape of the donor LE state would differ from its monomer due to electron donation into the triazine acceptor.

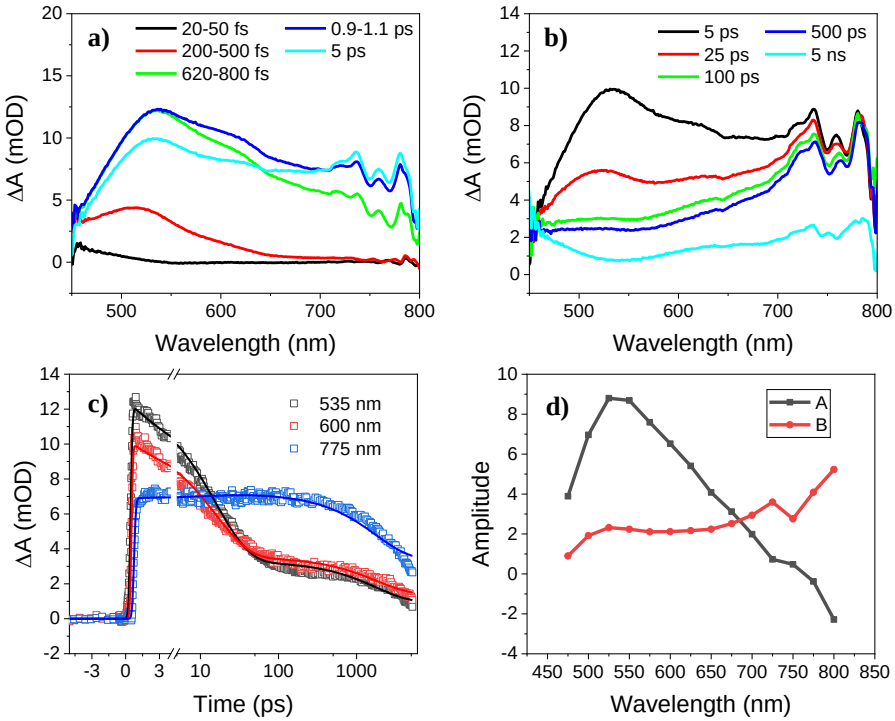

Figure 2.4. (a) and (b) Femtosecond TA-spectrum of pTCT at 340 nm excitation. (c) Fitted Kinetic Traces of TA spectra at given wavelengths; (d) Species-associated difference spectra derived from Global Fitting Analysis

Manifestation of several positive features on the spectra complicates the design of kinetic model for the ES dynamics of pTCT. For this reason, global fitting analysis of the TA spectra was performed in order to resolve the peaks. The kinetic trace of pTCT was fitted into bi-exponential decay function convoluted with Instrument Response Function (IRF), which results into two time constants: τ_1=15.67 ps and τ_2 = 1778 ps (**Figure 2.4c**). The global fitting also derives amplitudes of pre-exponential coefficient that can be associated with spectral characteristics of each ES. As can be seen, the ESA centered at

~525 nm can be assigned to LE state, whereas positive feature at >700 nm is attributed to exciton resulting from CT process (**Figure 2.4d)**. The kinetic trace shows that decay of 525 nm band does not lead to increase in the population of 725 and 775 nm bands. Therefore, the transition LE → CT can be excluded from the possible mechanism. In fact, they all undergo decay at later time: LE state (525 nm) decays fast, which validates its relatively short lifetime (τ_1=15.67 ps), while CT state is longer lived and quenches slowly with decay time of τ_2 = 1778 ps. Overall, the species-associated difference spectra (SADS) (**Figure 2.4d)** is consistent with the TA spectrum of pTCT, which confirms the validity of lifetimes and extinction coefficients of excited states.

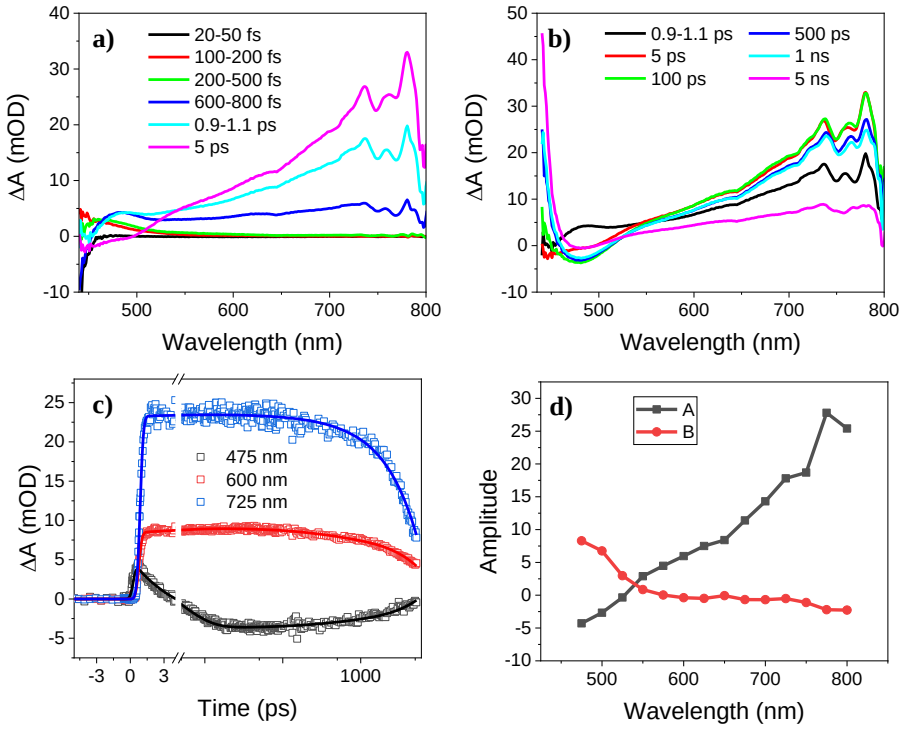

Figure 2.5. (a) and (b) Femtosecond TA-spectrum of pTCT-P at 340 nm excitation. (c) Fitted Kinetic Traces of TA spectra at given wavelength; (d) Species-associated difference spectra derived from Global Fitting Analysis

The addition of one phenylene ring between donor and acceptor significantly changes the spectral feature. In the TA spectra of pTCT-P, we observe the immediate formation of ESA centered at 475 nm at early time (<1 ps) following 340 nm excitation (**Figure 2.5a**). After that, the ESA decays, which is accompanied by the formation of a negative feature at the same region and a broad positive feature at > 650 nm (~1 – 100 ps, **Figure 2.5b**). The 475 nm negative feature resembles the steady-state emission of pTCT-P and can thus be attributed to SE due to population inversion after excitation. The positive feature > 650 nm is similar to that observed in the TA spectra of pTCT and can be assigned to the CT state. The difference of CT state between pTCT and pTCT-P mainly result from the intensity, where positive feature > 650 nm in the latter has much higher intensity than the immediately formed ESA at shorter wavelength. Global fitting analysis of the kinetics at different wavelength (**Figure 2.5c**) confirms the presence of two species involved in the ES processes (**Figure 2.5d**). First exciton shows maximum molar absorptivity peaking at 550 nm with decay lifetime of 4.509 ps. The second exciton, which was characterized as CT state decays slower with a lifetime of 3797 ps, which is longer compared to CT state of pTCT.

As donor and acceptor are separated further apart by two phenylene rings in pTCT-2P, the ES dynamics and CT process change significantly. The TA spectra of pTCT-2P (**Figure 2.6a and 2.6b**) shows a sharp peak centered at ~500 nm that grows until ~1ps and almost completely decays within ~5 ns. This peak differs significantly from the shape of the donor peak and resembles the known acceptor signal at ~475 nm (**Figure 2.3**). The red shift of this feature to 500 nm in pTCT-2P from 475 nm in the acceptor might be attributed

to the presence of biphenyl bridge in pTCT-2P, which extends the π-conjugation than monomer.

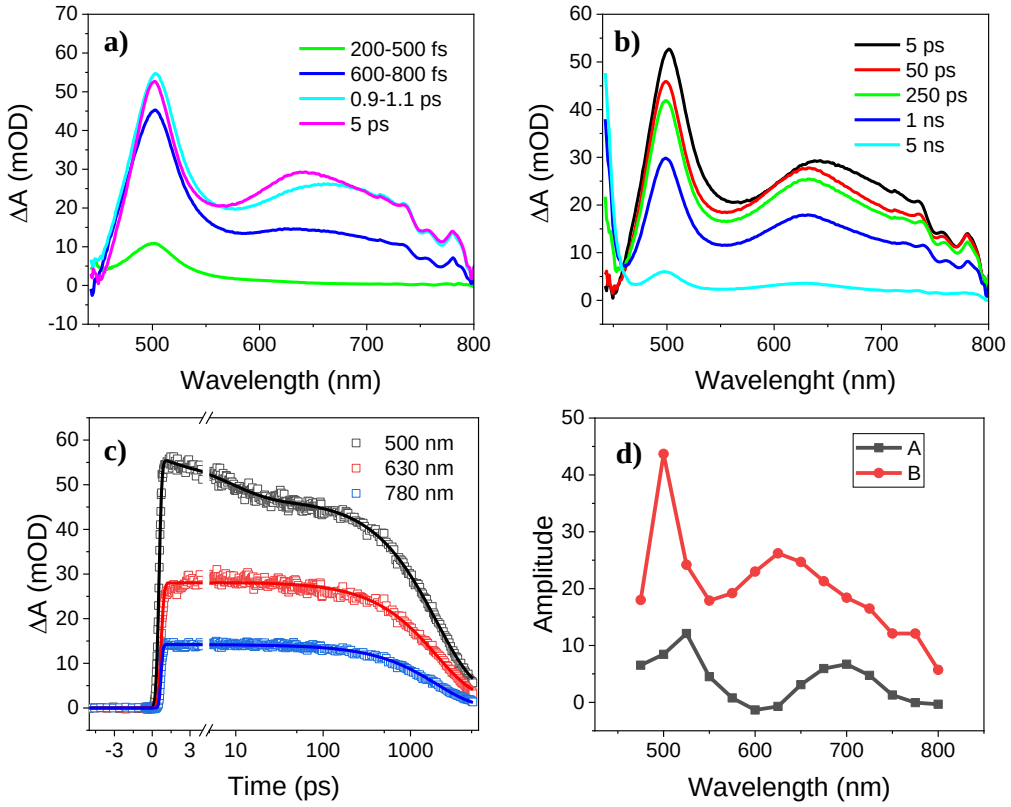

Figure 2.6: (a) and (b) Femtosecond TA-spectrum of pTCT-2P at 340 nm excitation. (c) Fitted Kinetic Traces of TA spectra at given wavelength; (d) Species-associated difference spectra derived from Global Fitting Analysis

This absorption is accompanied by the slightly delayed growth of a peak centered at ~650 nm which decays afterwards. The peak is similar to the double-lump feature at 600 and 650 nm in the TA spectrum of the acceptor, and can thus be attributed to the CT state formed through electron transfer from phenylene ring to triazine moiety (**Figure 2.3**). The intense CT absorption at > 700 nm which was observed in both pTCT and pTCT-P was barely observed in the spectra of pTCT-2P, suggesting that CT state is quite weak in pTCT-2P. The weak CT state in pTCT-2P might be explained by that the presence of large

spatial separation between the donor and acceptor by biphenyl rings leads to weak electronic coupling of donor HOMO orbital (carbazole) and acceptor LUMO orbital (triazine), where the CT state characteristic of 650 nm absorption corresponds to CT localized in the biphenyl bridge or from phenylene bridge to triazine acceptor. The molecular dynamics of pTCT-2P is fitted into bi-exponential decay function. The 500 nm band increases within ~1 ps followed by rapid decay with the overall lifetime of 8.885 ps. The quenching of 650 nm band seems to decay slowly after photoexcitation. This is also supported by its decay time of 1999 ps. Based on the dynamics, no transition between the states is observed.

Based on the analysis of TA spectra for pTCT, pTCT-P and pTCT-2P the rates associated with exciton dynamics can be expressed using the following Kinetic model:

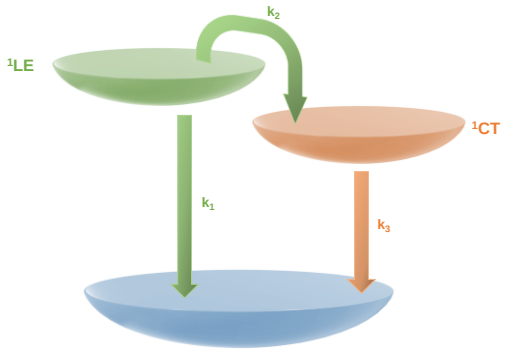

$$\frac{d[LE]}{dt} = -k_1[LE] - k_2[LE] = -(k_1 + k_2)[LE]$$

$$[LE] = N_0 e^{-(k_1+k_2)t}$$

$$\frac{d[CT]}{dt} = k_2[LE] - k_3[CT]$$

$$\frac{d[CT]}{dt} + k_3[CT] = k_2[LE]$$

$$[CT] = e^{-k_3 t}\int_0^t k_2 N_0 e^{-(k_1+k_2)t} e^{k_3 t}\, dt = e^{-k_3 t}\int_0^t k_2 N_0 e^{-(k_1+k_2-k_3)t}\, dt$$

$$= -\frac{k_2}{k_1+k_2-k_3} N_0 e^{-k_3 t} e^{-(k_1+k_2-k_3)t}\Big|_0^1$$

$$= -\frac{k_2}{k_1+k_2-k_3} N_0 e^{-k_3 t}\left(e^{-(k_1+k_2-k_3)t} - 1\right)$$

$$= -\frac{k_2}{k_1+k_2-k_3} N_0\left(e^{-(k_1+k_2)t} - e^{-k_3 t}\right) = k' N_0\left(e^{-(k_1+k_2)t} - e^{-k_3 t}\right)$$

$$[\boldsymbol{LE}] = \boldsymbol{N_0 e^{-(k_1+k_2)t}}$$

$$[\boldsymbol{CT}] = \boldsymbol{k' N_0\left(e^{-(k_1+k_2)t} - e^{-k_3 t}\right)}$$

$$\Delta A(\lambda, t) = \varepsilon_{LE}[LE] + \varepsilon_{CT}[CT] - \varepsilon_0([LE] + [CT]) = (\varepsilon_{LE} - \varepsilon_0)[LE] + (\varepsilon_{CT} - \varepsilon_0)[CT]$$

$$= (\varepsilon_{LE} - \varepsilon_0) N_0 e^{-(k_1+k_2)t} + (\varepsilon_{CT} - \varepsilon_0) k' N_0\left(e^{-(k_1+k_2)t} + e^{-k_3 t}\right)$$

$$\frac{\Delta A(\lambda, t)}{N_0} = (\varepsilon_{LE} - \varepsilon_0) e^{-(k_1+k_2)t} + (\varepsilon_{CT} - \varepsilon_0) k'\left(e^{-(k_1+k_2)t} + e^{-k_3 t}\right)$$

$$\frac{\Delta A(\lambda, t)}{N_0} = [(\varepsilon_{LE} - \varepsilon_0) + (\varepsilon_{CT} - \varepsilon_0) k'] e^{-(k_1+k_2)t} + (\varepsilon_{CT} - \varepsilon_0) e^{-k_3 t}$$

This supports that kinetic traces follow bi-exponential decay function.

While CT state between the donor and acceptor was observed in the TA spectra of both pTCT and pTCT-P, there are distinct difference between these two samples including the intensity and lifetime. The intensity which reflects the concentration of CT state is larger in pTCT-P than pTCT. Moreover, the formation time of CT state (4.509 ps) is faster while the lifetime of CT state is longer for pTCT-P molecule (3797 ps) than that for pTCT (1778 ps). In contrast, the CT state for pTCT-2P is much weaker than in pTCT. This was

further supported by excitation spectrum, which showed that for pTCT-P the major contribution for emission came from the CT state, while for pTCT and pTCT-2P both LE and CT states are responsible for radiative relaxation with relatively equal amount (**Figure 2.8)**. The possible reason for faster formation of more stable CT state in pTCT-P can be attributed to its D-B-A geometry. **Table 1** summarizes intrinsic time constants obtained from fitting procedure. The lifetime of LE carbazole moiety is shown as τ_1 for pTCT and PTCT-P, while for pTCT-2P it represents LE of biphenyl bridge between D and A. τ_2 represents decay time of CT state from carbazole to triazine for pTCT and from phenylene ring to triazine for pTCT-2P.

Table 2.1. Decay time of excited states in TCT series molecules

Time Constant	pTCT	pTCT-P	pTCT-2P
τ_1 **(LE)**	15.67 ± 1.11 ps	4.509 ± 0.8776 ps	8.885 ± 1.596 ps
τ_2 **(CT)**	1778 ± 461 ps	3797 ± 828.2ps	1999 ± 277.7ps

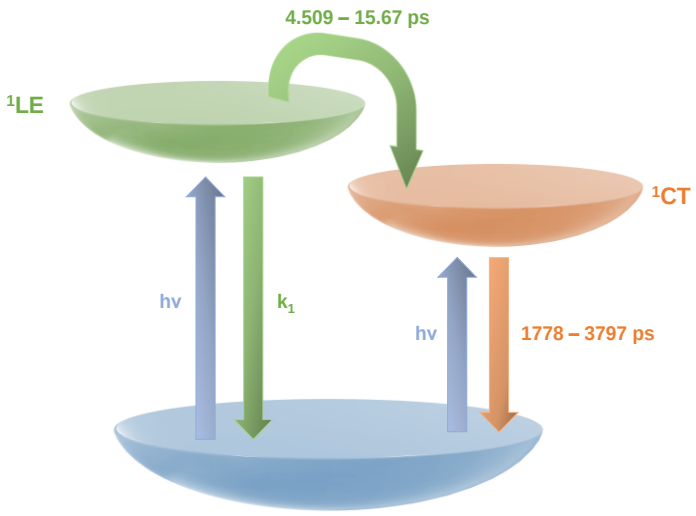

Scheme 2.2. The mechanism of the excited states in pTCT series molecules

These LE and CT states are likely the singlet states (^{1}LE and ^{1}CT) as the presence of oxygen has negligible impact on the emission lifetimes of these samples measured by time correlated single photon counting technique (TCSPC) (**Figure 2.8**). The overall ES dynamics of these star-shaped pTCT series is summarized in **Scheme 2.2**. The photoexcitation of these molecules results in the simultaneous formation of ^{1}LE and ^{1}CT states, which is then followed by a rapid non-radiative decay of ^{1}LE to ^{1}CT. The molecules eventually return back to the ground state and start decaying at different rate, where the decay of the ^{1}CT state is slower than decay of the ^{1}LE state (**Table 2.1**, **Scheme 2.2)**.

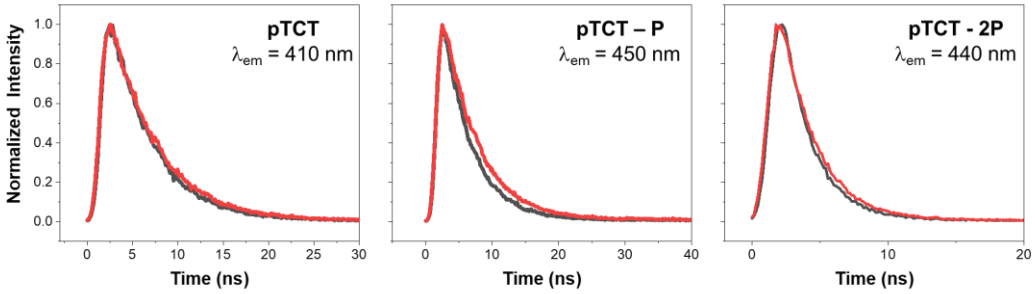

Figure 2.7. Time-resolved luminescence traces of TCT pTCT series molecules in toluene at room temperature under different atmospheres. N_2 (red) and air purging (black) for 15 min.

2.4. Conclusion.

Star-shaped donor-bridge-acceptor molecules have recently begun to attract interest due to an ability to undergo two-photon absorption, their potential to deliver better performance in OLED devices and significant promise as photocatalysts. Developing a full understanding of their photophysical behavior is necessary in order to incorporate rational design elements to this class of molecules. In this work, we report a systematic photophysical study on a series of triazine-phenylene-carbazole star-shaped D-B-A

molecules with 0, 1 and 2 bridging phenylene units using the combination of steady-state and time-resolved spectroscopy and time dependent density functional theory (TD-DFT) calculation. We show that the excited state relaxation pathways of these molecules are significantly dependent on the length of the bridge unit which governs the ground state torsional angles, excited state conformational relaxation, transition participation from the conjugated π-orbitals, along with electron/hole localization and effective electron/hole separation. Particularly, we were able to uncover and explain stimulated emission in a one phenylene bridged star-shaped D-B-A molecule resulting from a small conformational relaxation in the excited state due to effective electron/hole separation. Furthermore, we were able to uncover that longer bridging units are non-innocent which prevents effective electron-hole separation and is unable to prevent fast electron-hole recombination.

CHAPTER III: PHOTOPHYSICAL PROPERTIES OF BTPA-BASED IMINE-LINKED COVALENT ORGANIC FRAMEWORKS (COFs)

3.1. Introduction

Over last five decades, porous materials, such as zeolites, activated carbon and silica have shown great application in industry as catalysts and catalyst supports due to their large surface area and pore sizes allowing permeability of liquids and gases. [88–90] However, these porous compounds are lacking chemoselectivity, which is required for most catalytic processes.[91] In order to achieve such selectivity, a new class of porous materials with controlled functionality and structure have been developed. These include microporous (< 2 nm pore diameter) and mesoporous (2-50 nm pore diameter) materials, such as metal-organic frameworks (MOFs) [92–94] or porous coordination polymers (PCPs), covalent organic frameworks (COFs)[22,26,95] and porous organic frameworks (POFs)[25,96]. The thermodynamically controlled polymerization leads to periodically ordered crystalline networks with nonuniform pores.[91]

The advantages of COFs include low cost, light weight, stability, structural diversity and tunability.[92] This means that the properties and implementation of COFs can be easily modified by altering the building block molecules or their functional groups. Moreover, structural modifications allow tunability of pore sizes of COFs in order to capture toxic chemicals, gases and solvents.[96] These properties of porous materials make them practical for storage of carbon dioxide,[97,98] methane,[99] hydrogen,[100] adsorption and encapsulation of dyes or organic solvents. [101,102] Besides, donor-acceptor (D-A) based architecture of some COFs can adopt charge transfer (CT) state leading to electron-hole pair formation and

absorption of visible light allowing them to be useful in photocatalysis for oxidation of sulfides[103] and amines[104], generation of hydrogen,[6,105] etc.

As COF samples possess crystalline structure, the individual sheets of COF samples can create stacks, which facilitate coupling of π-orbitals.[29,106–108] The formation of such π-conjugated system of COF layers leads to electron delocalization under photoexcitation.[23,106] As has been previously reported in the literature, the electron transfer (ET) between D and A units can proceed further by delocalization of this charge between D-A blocks arranged perpendicular to each other.[23,24,63] Hence, the efficient interlayer CT process in organic frameworks can result in long-lived CS state and allow the use of these materials as transistors, light emitting diodes and photodiodes.[63,106,109] Since the further application of COFs can be associated with its ability to generate delocalized electron throughout the expanse of its framework, it is crucial to build a basic understanding of how this process happens.

Currently a plenty of research was accomplished on the synthesis[110,111] and pore size control[112,113], application of COFs for gas storage, [97–100] adsorbents[96] and photocatalysts.[6,103–105] However, the optical and photophysical properties of D-A COFs were not elucidated in great extent. In this work, the optical properties were investigated using steady-state spectra as well as femtosecond transient absorption (TA) Spectroscopy. This provides information on the excited state dynamics of COF samples, which elucidates the mobility of charge along the structure and possibly between successive sheets. Here, we show the photophysical properties of three synthesized COFs (**TPB-COF, TPA-COF** and **TPT-COF, Scheme 3.1**), which were synthesized using a repeat units of **BTPA** (5,5',5"-(1,3,5-Benzenetriyl)tris[2-pyridinecarboxaldehyde]) and a series of three different

organic precursors: 1,3,5-Tris(4-aminophenyl)benzene (**TPB**), 4,4',4''-Triaminotriphenylamine (**TPA**), and 1,3,5-Tris(4-aminophenyl)triazine (**TPT**). These precursors differ in the electron affinity and therefore, synthesized COFs are expected to have lowered energy band gap and generate the CT state upon photoexcitation.[24,114,115] Our studies show the formation of polariz star-shaped carbazole-π-triazine organic chromophores ed state in the time scale between 1.06 to 1.86 ps and that CS between D and A can live up to 588.8 ps. Moreover, it indicated that the role of BTPA as electron accepting group changes when it is coupled with TPB and TPT, as the TA spectra show charge density in the excited state is directed and fixed in these (TPB and TPT) units, when CT state is formed.

3.2. Experimental

Film preparation. 1-2 mg of TPB-COF, TPA-COF and TPT-COF was dispersed in 5 ml ehtnaol and 100 μL of Nafion^{TM}. The mixture was sonicated for 3 hours to create homogeneous distribution of COF crystals. The suspension was then coated on a quartz substrate and left to allow solvent to evaporate for 24 hours.

Standard characterization. UV-visible absorption measurements were carried out using Agilent Cary 5000 UV-vis-NIR spectrometer using as prepared PcCu and PcNi COF samples on quartz substrate.

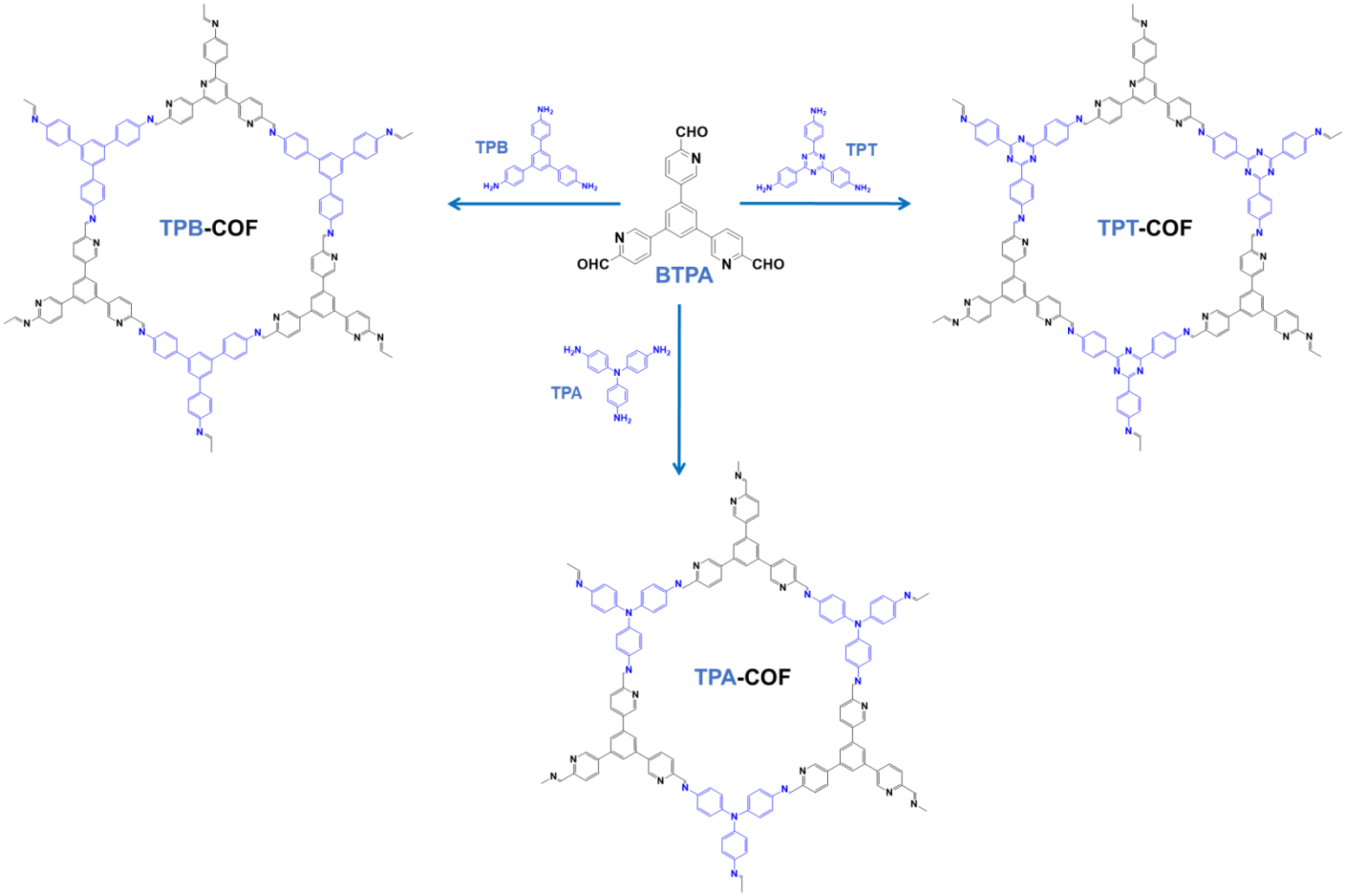

Scheme 3.1. Chemical structure of precursors and TPB-COF, TPA-COF and TPT-COF

For steady-state absorption and luminescence measurements, the suspension of TPB-COF, TPA-COF and TPT-COF in ethanol was used. The suspension was prepared my dispersing ~2 mg of TPB-COF, TPA-COF and TPT-COF in 25 ml anhydrous ethanol and sonicating it for 24 hours. Samples were placed in 10 mm quartz cuvettes (Starna). UV-visible absorption measurements were carried out using Agilent Cary 5000 UV-vis spectrometer. Steady state luminescence data were obtained on a PTI QM40 Spectrophotometer implemented with 75 W Xenon Lamp as excitation source and controlled by Felix GX Software.

Transient Absorption Spectroscopy. As discussed in Chapter II, Femtosecond Transient Absorption experiments were performed on a Helios Spectrometer (Ultrafast Systems LLC). The pump and probe pulses were generated using Ti:Sapphire laser system (Solstice, 800nm, 3.5 mJ/pulse, 1 KHz repetition rate). Pump is delivered from TOPAS using 75% yield of Ti:Sapphire laser chopped at 500 Hz. The generation of white light continuum (probe) takes place using 25% output of the amplifier and sapphire crystal.

TPB-COF, TPA-COF and TPT-COF film on quartz substrates were placed to sample holder and continuously translated in order to prevent heating and thermal degradation. The measurements were collected at 400 nm pump pulse with 350 μW pump power.

3.3. Results and Discussion

Standard Characterization

Solid-state absorption spectra of TPB-COF, TPA-COF and TPT-COF were measured using diffuse reflectance spectroscopy. As shown in **Figure 3.1**, TPB-COF,

TPA-COF, and TPT-COF show broad absorption in the visible region (extends to > 600 nm) with maximum at 425 nm, 580 nm, and 415 nm, respectively. The reflectance is bathochromic with respect to absorption spectra of precursors for TPB-COF and TPT-COF, suggesting the formation of charge transfer (CT) state due to increasing degree of conjugation between BTPA with TPB and TPT. To gain insight on the contribution of interlayer interaction to the broad absorption spectrum, the COF samples were exfoliated to create separate 2D sheets. The normalized absorption and luminescence spectra of COF samples in ethanol were also shown in Figure 1b. It is interesting to note that the maximum absorption for TPB-COF (410 nm) and TPA-COF (515 nm) in ethanol retained while the maximum absorption of TPT-COF at 405 nm which was present in solid sample (**Figure 3.1**) is suppressed in ethanol suspension (**Figure 3.2a**). This may suggest that the absorption at 405 nm in solid state TPT-COF results from the interlayer CT. The possible explanation for the observed interlayer CT in TPT-COF can result from that its relatively planar geometry allows greater stacking of successive layers, which leads to higher charge delocalization between TPT-COF layers. Higher energy peak located in UV region agree well with the absorption spectrum of the corresponding linkers and thus can be attributed to the local absorption from the linkers.

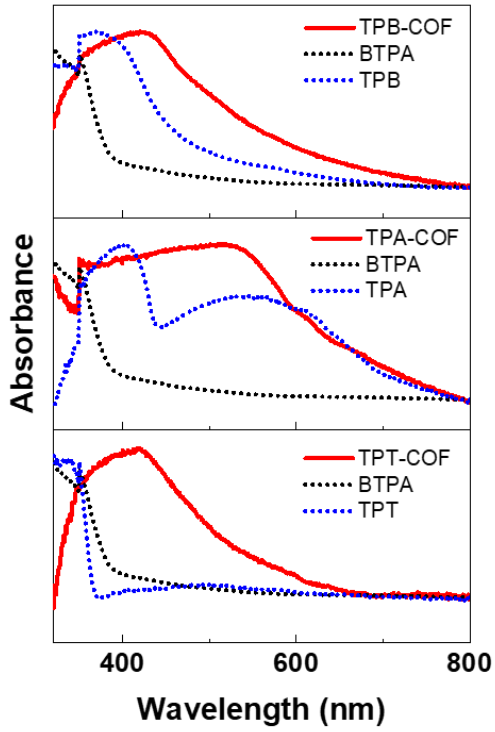

Figure 3.1. Diffuse reflectance spectra of TPB-COF, TPA-COF and TPT-COF recorded in the solid state

Based on the photoluminescence spectra collected at 310 nm excitation, the COF samples are not strong emitters. The intensities of TPB-COF and TPA-COF reach ~$5.5 \cdot 10^5$ counts, while for TPT-COF it is ~$1.55 \cdot 10^5$ counts. The reason for such low photoluminescence intensity can be extremely low concentration of COF samples in ethanol, as the majority of the amount dissolved precipitates. Weak emission can be also seen from the image of COF samples under UV-lamp on the **Figure 3b**. The emission maximum is Stokes-shifted with respect to absorption maximum in UV region, but overlaps with absorption in visible region. The photoluminescence of TPB-COF appears at 435 nm, which is 10 nm red-shifted compared to emission from TPB and for TPT-COF emission stretches between 350 and 450 nm corresponding to 375 nm fluorescence in TPT.

On the other hand, for TPA-COF the emission is 55 nm blue-shifted compared to TPA and appears at 380 nm. Therefore, photoluminescence is produced due to radiative relaxation from LE state. The excitation of these molecules at 400 and 500 nm does not result in an emission.

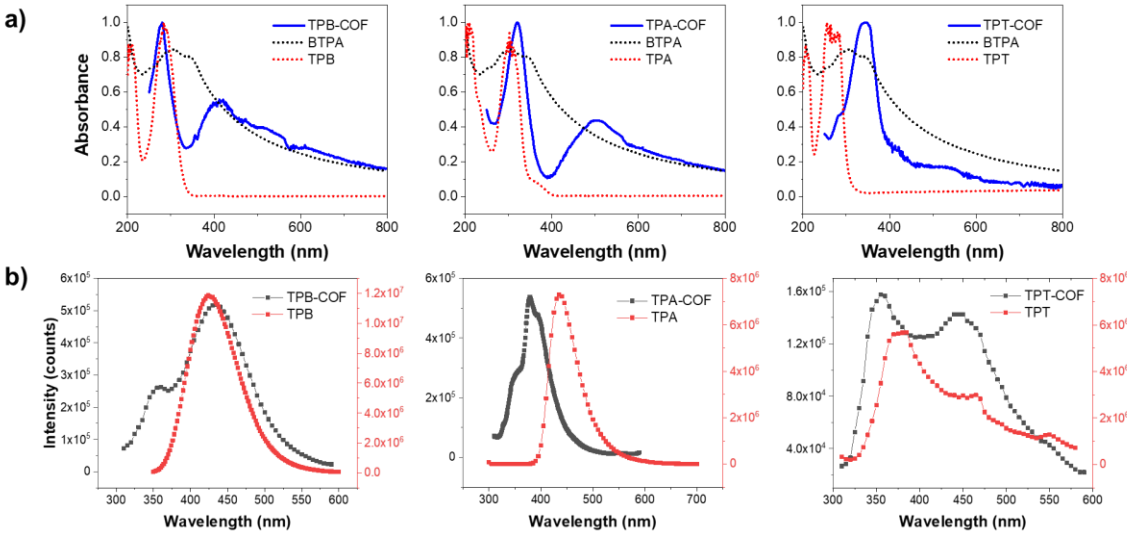

Figure 3.2. (a) Normalized steady-state absorption of TPB-COF, TPA-COF, and TPT-COF with the constituting precursor molecules, (b) Comparison of photoluminescence emission spectra of COF samples with the precursors

Transient Absorption Spectroscopy

The excited state dynamics of these COFs was examined by transient absorption (TA) spectroscopy following 400 nm excitation. As shown in **Figure 3.3a**, the TA spectra of TPB-COF were featured by a negative feature centered at 490 nm and a broad excited state absorption (ESA) at > 550 nm. The former agrees well with the absorption edge observed at the diffuse reflectance spectrum and can thus be assigned to the ground state bleach (GSB) of TPB-COF. The broad ESA is also observed in the TA spectra of TPB (**Figure 3.3b**), suggesting that it originates from singlet excitons of the TPB cores in the TPB-COF.

The GSB and ESA have an isosbestic point at 549 nm and decay in the same manner (**Figure 3.4a)** suggesting that they represent the same relaxation pathway, i.e. returning to GS from ES. Similar spectral signatures are observed in the TA spectra of TPT-COF measured under 400 nm laser irradiation (**Figure 3.3c**), which displays negative band at 460 nm due to GSB and broad ESA at > 520 with isosbestic point at 515 nm. The same kinetics trace for GSB and ESA (**Figure 3.4b**) suggesting a simple relaxation dynamics from ES to GS.

The TA spectra of TPA-COF upon 400 nm photoexcitation (**Figure 3.3e**) exhibit an ESA centered at ~475 nm and a negative band centered at 675 nm. The absorption profile at ~475 nm yields similar feature with the ESA at around 500 nm of BTPA spectra (**Figure 3.3f**), suggesting local excitation of BTPA moiety in the framework. The negative feature can generally either be attributed to the GSB or stimulated emission (SE). Because the diffuse reflectance spectrum of TPA-COF shows absorption edge of ~700 nm while negligible emission was observed in the emission spectrum of TPA-COF suspension in ethanol, we conclude that this negative feature can be attributed to the GSB of TPA-COF. Interestingly, the diffuse reflectance of TPA generates broad absorption feature centered at 600 nm, which may suggest that this bleach signal is associated with the hole formation in electron donating TPA core. It is more interesting to note that the negative feature at 675 nm decays more slowly compared to the positive ESA at ~475 nm (**Figure 3.4c**). This may be explained as the relaxation from the local excited BTPA to the formation of exciton with electron in BTPA core and hole in the TPA.

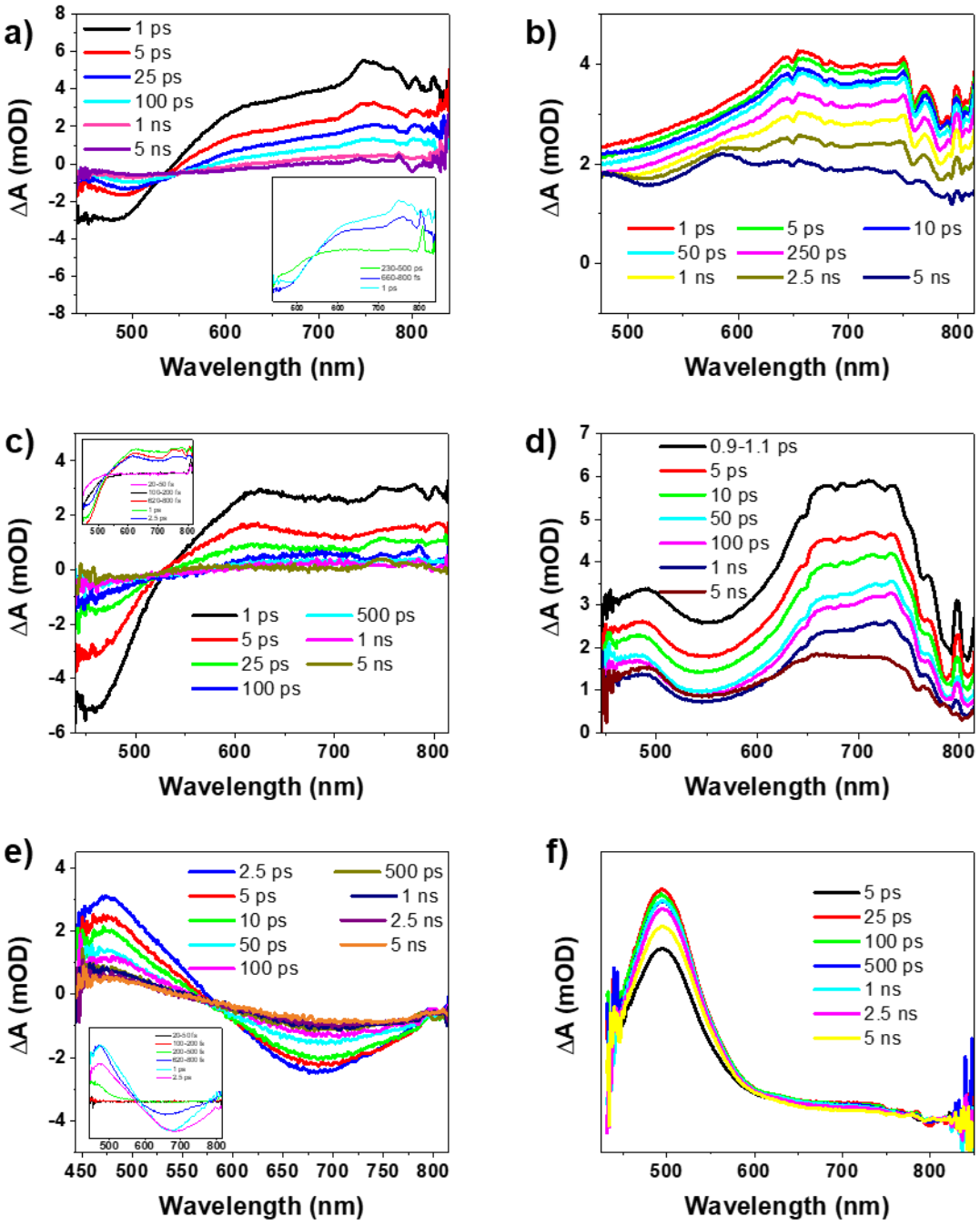

Figure 3.3. Transient absorption spectra of COF samples at 400 nm excitation and precursors at 320 nm excitation: (a) TPB-COF, (b) TPB, (c) TPT-COF, (d) TPT, (e) TPA-COF, and (f) TPA

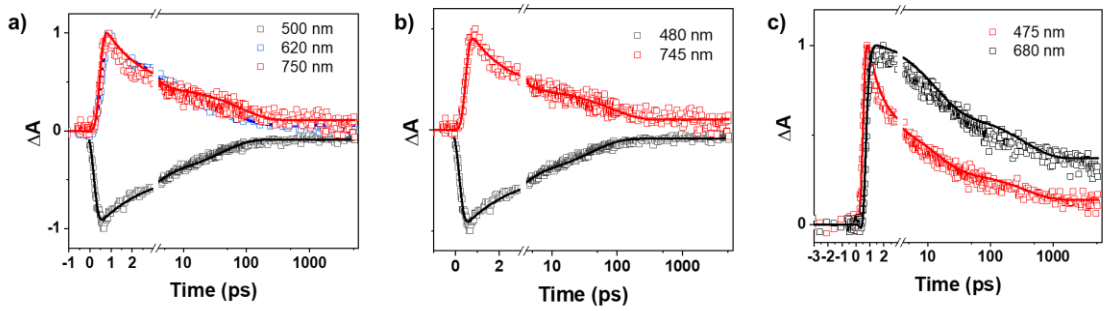

Figure 3.4. Kinetic decay profiles of (a) TPB-COF, (b) TPT-COF, (c) TPA-COF

The kinetic traces of COF samples were normalized to the maximum intensities and analyzed using Global Fitting. The best fit of the transient signals at representative wavelengths (**Figure 3.4a-c**) was obtained using three exponential decay dynamics with the lifetimes reported in **Table 3.1**. Shortest lifetime (τ_1) corresponds to the CT from D to A, whereas the lifetimes in hundreds picosecond range (τ_3) can be assigned to charge recombination and relaxation from CT state to ground state (**Scheme 3.2**). TA spectra showed that for TPB- and TPT-POFs the CT process takes place in the direction towards TPB and TPT correspondingly (**Scheme 3.2a**). In case of TPA-COF, TPA unit is electron-rich and therefore acts as a donor. Moreover, the electron affinity difference between TPA and BTPA appears to be the largest, as the charge recombination requires more time (2622 ps) compared to the other two samples (**Scheme 3.2b**).

Table 3.1. Exciton lifetimes of TPB-COF, TPA-COF and TPT-COF

Time Constant	τ_1	τ_2	τ_3
TPB-COF	1.86 ps	30.79 ps	588.8 ps
TPA-COF	8. 26 ps	51.48 ps	2622 ps

TPT-COF	1.29 ps	16.84 ps	407.5 ps

Scheme 3.2. Excited state dynamics in (a) TPB-COF and TPT-COF, (b) TPA-COF

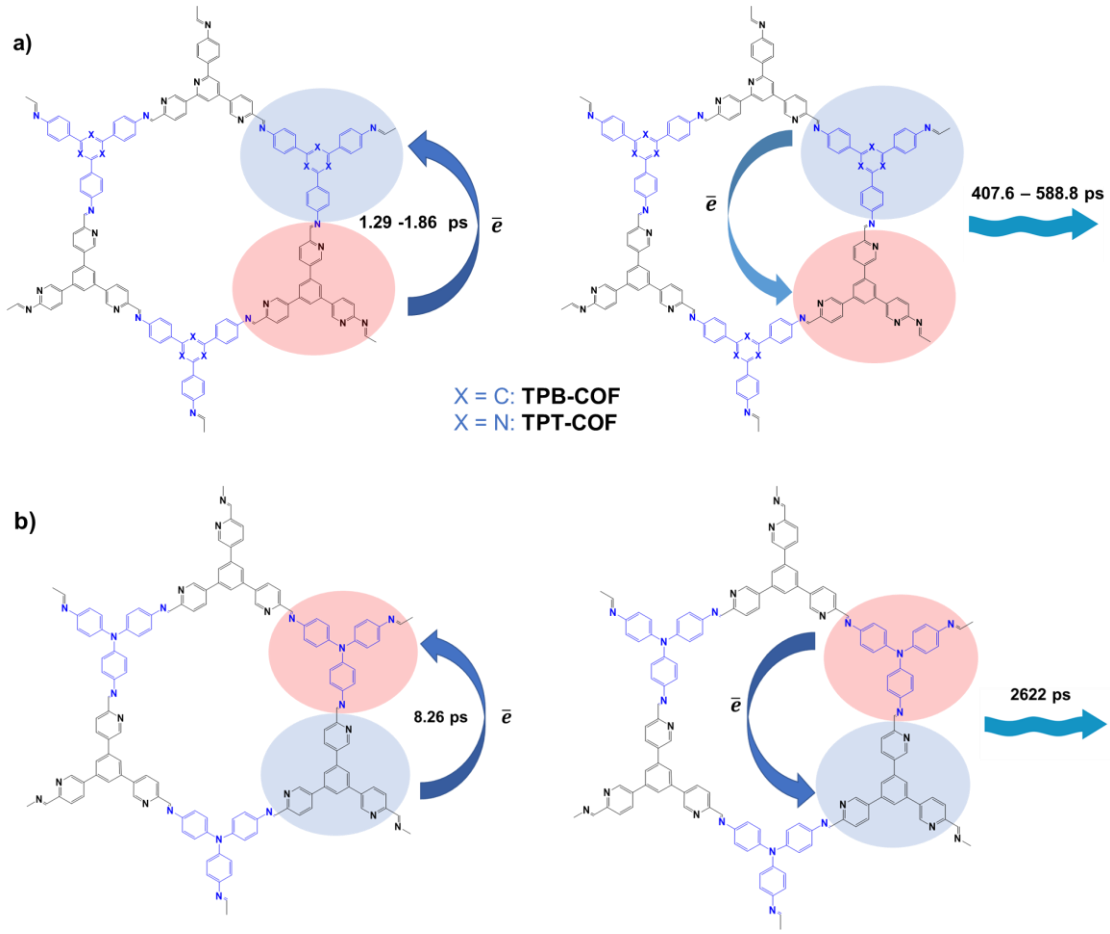

3.4. Conclusion

In summary, the photophysical properties of three donor-acceptor COFs were investigated using time-resolved TA spectroscopy. The results show in the TPB-COF and TPT-COF the relative electron affinity of BTPA compared to TPB and TPT is higher and therefore, it acts as an electron donating unit. The electron migration from BTPA to π-conjugated TPB, TPT units was detected as broad excited state absorption for TPB-COF and TPT-COF. The opposite was observed in the TA spectra of TPA-COF, which showed

charge separation between oxidized TPA and reduced BTPA units. In the TA spectra of TPA-COF a characteristic BTPA ESA was observed along with GSB from TPA unit, featuring charge separated state $TPA^{+\bullet}$ - $BTPA^{-\bullet}$. Kinetic traces indicated that strongest electron affinity difference between TPA and BTPA also resulted in the most long lived charge-separation state that can be determined within the time window of our instrument. The charge recombination process is almost five times longer (2622 ps) for TPA-COF compared to TPB- and TPT-COFs (407.6 – 588.8 ps) due to larger difference in electron affinities and ionization potentials. The For better support, the voltammetry experiment can be conducted in order to determine electron donating and withdrawing potentials of the precursors.

CHAPTER IV: CHARGE DYNAMICS IN DONOR-ACCEPTOR METALLOPHTHALOCYANINE COVALENT ORGANIC FRAMEWORKS (COFs)

4.1. Introduction

Covalent organic frameworks (COFs) consisting of the assembly of periodically arranged donor-acceptor heterojunctions demonstrates practical application as organic semiconducting materials, light-emitting diodes and transistors.[27,34–41] Structural modification of COFs allows the tunability of optical bandgaps between frontier molecular orbitals, which is useful in the design of organic semiconductors.[116] Moreover, the low cost of organic electronic material promises the development of economically viable solar cells.[117] A number of existing studies in the literature have examined semiconducting and photoconductive properties of arene, porphyrin and phthalocyanine COFs due to their ability to create π-columnar array during thermodynamically controlled polymerization.[36,37,118–125]

Jiang *et.al*. synthesized a series of COFs consisting of various methallophthalocyanine donor and diimide acceptor units.[23,34,63] It was shown that the control of periodic arrangement of building blocks into two-dimensional (2D) structure along with the ordered stacking of COF layers induces the delocalization of free charge along the π-columns, inhibits rapid charge recombination and retains long-lived polarized state of COF.

The choice of methallophthalocyanine as an electron donating units in these COF samples can be explained by their high ionization potential due to 18π-electron aromatic molecular orbital system. In 1986 Tang used copper phthalocyanine and perylene tetracarboxylic dianhydride bisbenzimadizole to create the first two-layer organic photovoltaic cell.[127] Since then metallophthalocyanines were widely tested mostly in

conjunction with fullerene for the development of new class of organic photovoltaic devices.[128–131]

Herein, the charge dynamics in thin films of 2D COFs (**PcCu COF** and PcNi COF) constructed using ester-linked copper and nickel phthalocyanine and 2,3,5,6-tetrafluoroterephthalonitrile (**TFTPN**) is examined using time resoled spectroscopy (**Scheme 1**). UV-visible absorption measurements yielded characteristic absorption features of phthalocyanines at Soret and Q bands. As a result, Transient absorption (TA) spectrum was collected under photoexcitation at both 300 nm (Soret band) and 650 nm (Q band). The analysis of kinetic traces showed that the charge dynamics involves the electron density localization in phthalocyanine unit followed by the charge migration to proximate TFTPN. Within maximum 72.68 ps, the electron is transferred between COF layers and the charge recombination takes place after nearly 3 ns.

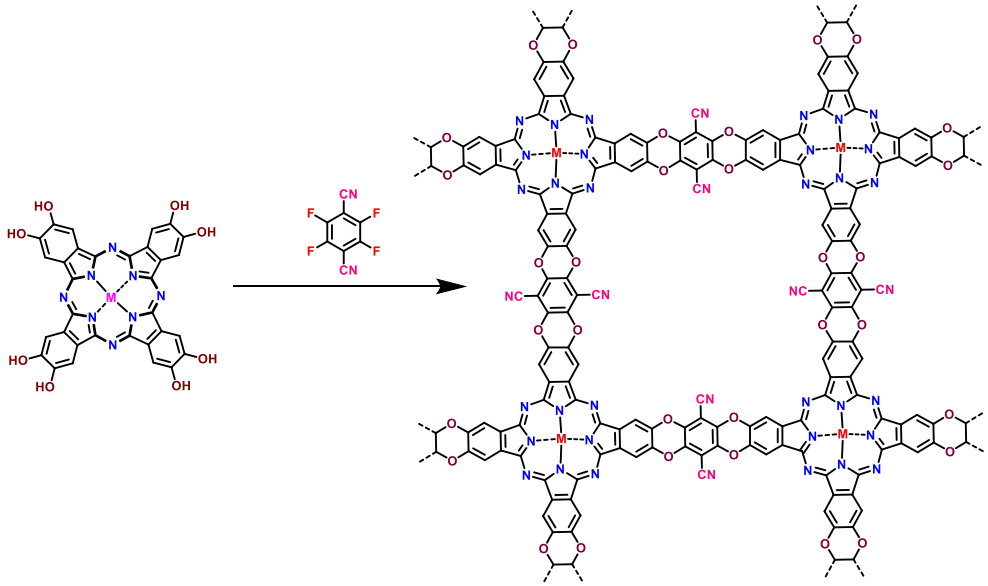

Scheme 4.1. The synthetic scheme for the formation of Metallophthalocyanine COF

4. 2. Experimental

Standard Characterization. UV-visible absorption measurements were carried out using Agilent Cary 5000 UV-vis-NIR spectrometer using as prepared PcCu and PcNi COF samples on quartz substrate.

Transient Absorption Spectroscopy. As discussed in Chapter II, Femtosecond Transient Absorption experiments were performed on a Helios Spectrometer (Ultrafast Systems LLC). The pump and probe pulses were generated using Ti-Sapphire laser system (Solstice, 800nm, 3.5 mJ/pulse, 1 KHz repetition rate). Pump is delivered from TOPAS using 75% yield of Ti:Sapphire laser chopped at 500 Hz. The generation of white light continuum (probe) takes place using 25% output of the amplifier and sapphire crystal.

PcCu and PcNi COF film on quartz substrate were placed to sample holder and continuously translated in order to prevent heating and thermal degradation. The measurements were collected at 300 nm and 600 nm pump pulse with 270 and 450 μW power respectively.

The kinetics data were fitted using Surface Xplorer Software by Ultrafast Systems LLC. Kinetic trace at a certain wavelength is expressed as fitting function which represents convolution of instrument response function (IRF) with exponential decay:

$$S(t) = e^{-\left(\frac{t-t_0}{t_p}\right)^2} * \sum_i A_i e^{-\frac{t-t_0}{t_i}}$$

$$t_p = \frac{IRF}{2ln2}$$

where t_0 is time zero, *IRF* is the half maximum width of instrument response function, A_i and t_i are the amplitude and decay constants respectively.

4. 3. Results and Discussion

Standard Characterization

Copper and nickel phthalocyanine groups absorb light in the visible region and have deep green color. Distinctive UV-visible absorption spectral image is observed for the COF sample arising from 18π-electron aromatic molecular orbital system overlapping with d-orbitals in the metal center. The steady-state UV-visible absorption spectra indicated typical Soret band (B band) attributed to the $\pi \rightarrow \pi^*$ transition. For PcNi COF the B zone appears as a sharp peak at 295 nm with a shoulder peak around 400 nm. The absorption feature of PcCu COF in the UV region is splitted to 285 and 345 nm bands.

Q band corresponds to excitation from ground state to the first singlet excited state stretching between 550 and 900 nm. The Q zone undergoes characteristic Davydov splitting for PcNi COF present in most phthalocyanine derivatives.[132,133] It appears at 635 and 697 nm for PcNi COF, while for PcCu the splitting is negligible and emerges at 645 and 700 nm. The broad absorption peak of PcCu COF can be the indication of symmetry reduction.[134] The slight red-shift of Q band compared to absorption of CuPc, which appears as double-lump at ~620 nm and 695 nm,[134] and NiPc (615 and 685 nm)[135] can be caused by linkage with TFTPN with higher electron affinity than CuPc and differences in aggregation patterns with the monomer.[116]

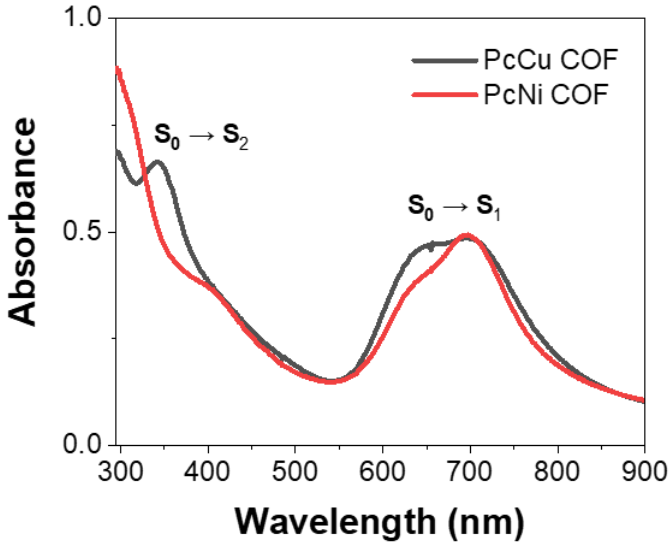

Figure 4.1. Steady-state absorbance spectra for PcCu and PcNi COFs

Photoluminescence measurements demonstrated no emission of solid PcCu and Pc Ni COFs under irradiation over visible region. This observation is consistent with the photoluminescence spectra of previously synthesized metallophthalocyanine COFs, which similarly displayed non-emissive properties. This can be characterized in term of formation of phthalocyanine cofacial H-aggregates that act as trapping sites.[116,136]

Transient Absorption Spectroscopy

Toward understanding the excited state processes of metallophthalocyanine organic framework, femtosecond TA spectroscopy was employed. Thin films of PcCu and PcNi COFs were irradiated first at 300 nm pulse to excite second singlet exciton (S_2). The positive transient signal centered at 550 nm along with negative ground state bleach stretching between 610 and 800 nm is observed in the TA spectra of PcCu COF. The bleaching signal is assigned to depopulation of ground state due to absence of any

stimulated emission in this region as was above-mentioned. The negative feature does not coincide with the shape of Q band absorption, which can signify an overlap with the excited state absorption in the region between 610 and 800 nm.[1,134] The decay profiles of the 550 and 650 nm features indicate similar decay rate with slow quenching starting from 1 ps. It is interesting to note that, the intensity of negative peak is almost 1.5 higher than the intensity of ESA under excitation at 300 nm.

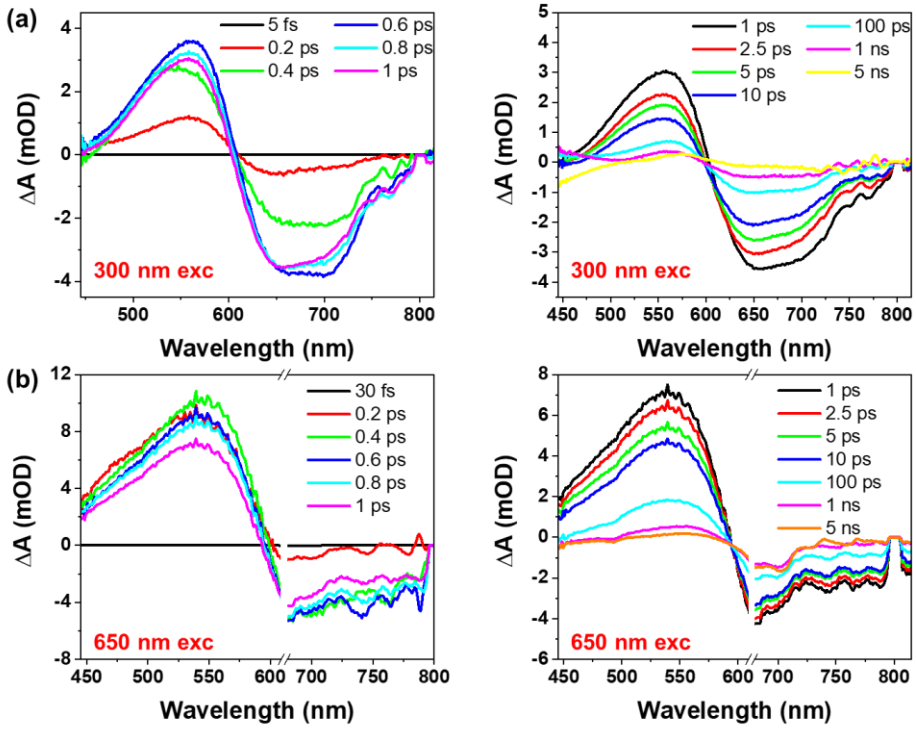

Figure 4.2. Transient absorption spectra of PcCu COF at (a) 300 nm (b) 650 nm laser irradiation

Similar optical signatures are observed for the TA spectra of PcNi COF excited using 300 nm pulse. The ESA signal appears at 560 nm and the bleaching signal is centered at 685 nm. Analogously, the overlapping of ground state bleach with ESA can be observed. Both signals gradually decay after 1 ps. Although the overall spectral image looks similar,

it must be pointed out that GSB for PcNi COF is almost twice more intense compared to positive absorption feature.

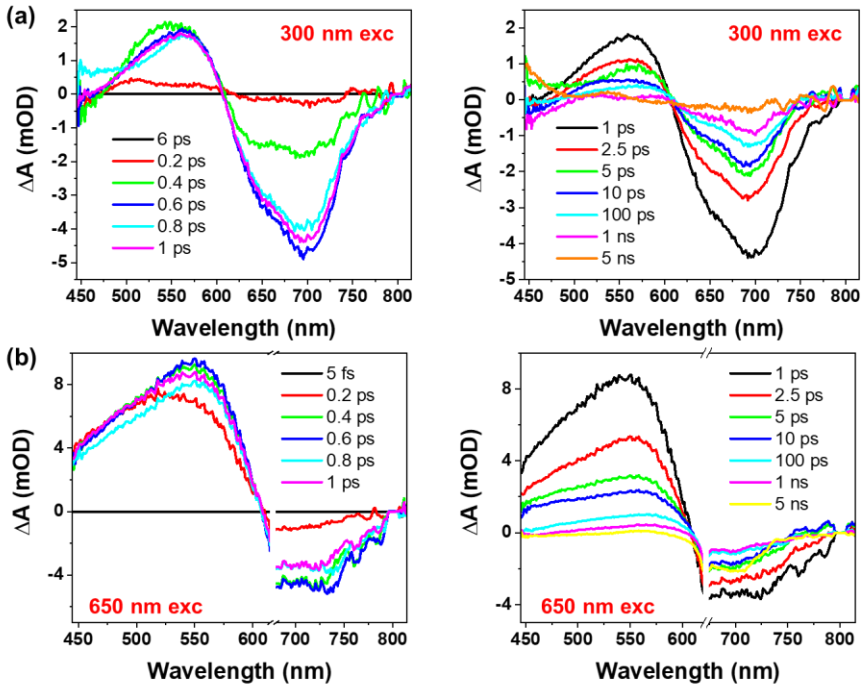

Figure 4.3. Transient absorption spectra of PcNi COF at (a) 300 nm (b) 650 nm laser irradiation

According to Kasha's rule, excitation of Soret band must be followed by internal conversion to lower electronic state.[137] In order to mimic this process, the TA data was obtained using 650 nm laser resulting in the excitation of Q band. A similar pattern of results was obtained displaying 550 nm ESA with significantly broadened negative absorption band for PcCu COF. The TA spectra of PcNi COF yields 560 nm induced absorption peak and broad bleaching signal analogously to copper version. The positive feature around 550 nm in both PcCu and PcNi COFs suggests that it can be assigned to ESA of S_1 state due to its presence upon 650 nm excitation. In contrast with excitation to B band, the TA spectra are dominated by threefold enhanced ESA due to direct pumping of molecules to the first singlet excited electronic state (S_1). Besides, relative intensity of

signals, the bands do not show any obvious shift upon Q band irradiation and overall, the TA spectra recorded at 300 and 650 nm wavelengths have almost similar optical profile. This implies that $S_2 \rightarrow S_1$ transition is not detected in the TA spectra of PcCu and PcNi COFs upon 300 nm excitation due to (a) absence of bleaching signal in the B band region and (b) no indication ESA corresponding to population of S_2 state (**Figure 4.4**).

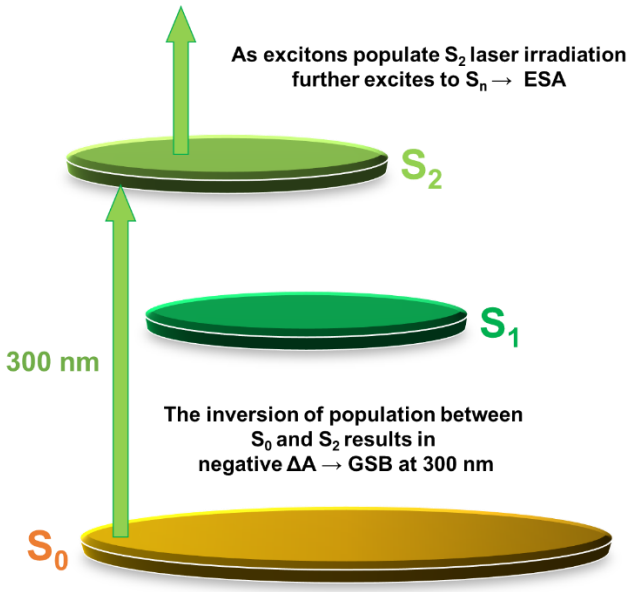

Figure 4.4. Potential energy diagram of electronic states of metallophthalocyanine units

There can be two possible explanations for the absence of both GSB and ESA. First, as can be seen from TA spectra at 300 nm excitation the positive induced absorption feature is apparent at 200 fs time delay. This may imply that the $S_2 \rightarrow S_1$ transition is ultrafast and can occur between 5 and 200 fs. It is also possible that the time constant for this transition is shorter than instrument response function (IRF) resulting in insensitivity of TA instrument to internal conversion between singlet excited states. Another possible explanation arises from the fact the GSB signal overlaps with positive absorption feature in longer wavelength region, which can suggest that this positive band is the characteristic

S_2 induced absorption. As the GSB dominates in this region as S_1 gets populated, as a result of internal conversion, the induced absorption smears through overlap with negative feature.

Overall, the TA spectra of PcCu COF is consistent with the previously reported TA spectra of copper phthtalocyanine vapor deposited film with nearly 40 nm bathochromic shift.[134] This observation is predictable due to the excitation of metallophthalocyanine unit and therefore, the photoinduced absorption and negative bleaching signal corresponds to local excitation of electron-donating part of the COF. The majority of the time-resolved TA spectroscopy on the metallophthalocyanine molecules and their derivatives indicated the formation of long-lived triplet state. The triplet state is formed within a picosecond and depending on the sample had a lifetime ranging from 8 ns to several microseconds.[63,134,138,139] In PcCu COF sample the excitons almost completely decays by 5 ns suggesting absence of triplet state. Therefore, such rapid quenching of locally excited copper phthalocyanine species can be introduced by electron withdrawing nature of TFTPN. The assembly of metallophthalocyanine-donor and TFTPN-acceptor in COFs results in the formation charge separated state ($PcCu^{+\bullet}$-$TFTPN^{-\bullet}$) preceded by locally excited copper phthalocyanine unit (PcCu*).

In the previous study by Jiang *et. al*. in 2015 related to metallophthalocyanine-diimide COFs they studied TA spectra of the samples dispersed in DMF in order to delaminate COF layers. Using atomic force microscopy, it was found that delamination in DMF generated COF samples with the thickness ranging between hundreds nanometers and 1 μm. Femtosecond TA spectra of this sample yielded that charge separated state is formed within 1.8 ps and its lifetime expands to 217 ps. The lifetime of charge separated

state showed dependence with the thickness of COF layers, which decreases as fewer sheets form π-columnar array.[23]

Our study on the solid film revealed that the excited state dynamics of COF is expressed as three-exponential decay function. The positive absorption at 550 nm for PcCu COF and 560 nm for PcNi COF decays relatively at the same rate independently from excitation wavelength (**Figure 4.5a** and **4.5b**). This suggests that the formation of locally excited (LE) state of electron-rich PcCu and PcNi unit is nearly equivalent under 300 nm and 650 nm laser irradiation. As LE state relaxes down electron transfer from metallophthalocyanine unit to the proximate TFTPN takes place. The excited state dynamics is then followed by delocalization of electron along donor-acceptor π-columns. Interlayer electron transfer of this type in J-aggregates[23,63] of COF is believed to suppress charge recombination process contributing to longer lifetime of $PcCu^{+\bullet}$-$TFTPN^{-\bullet}$ state. Hence, the donor-acceptor configuration of COF involves formation of charge-separated state, whereas the development of π-stacks of COF layers results in long-range migration of electron inhibiting charge recombination. It was reported in prior research that delocalization of charge along bicontinuous π-columnar array of zinc phthalocyanine and naphthalene diimide COF can be expressed as transient signal, which has a shape of negative mirror image relative to ground state absorption.[23,63]

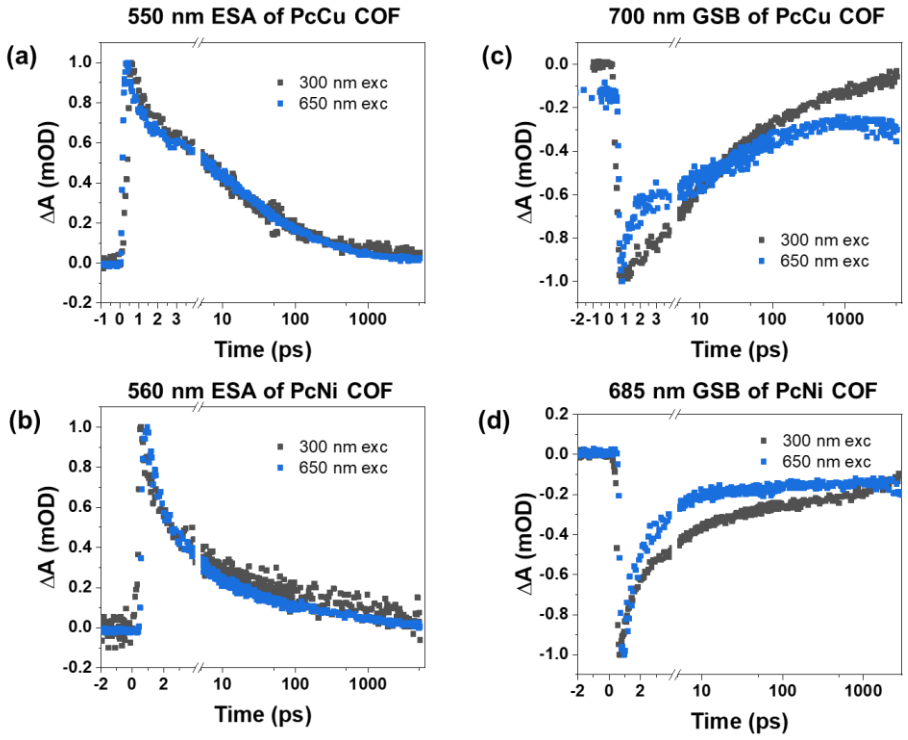

Figure 4.5. Kinetic decay profiles of (a) 550 nm band of PcCu COF, (b) 560 nm band of PcNi COF, (c) 700 nm band of PcCu COF, and (d) 685 nm band of PcNi COF

The kinetic trace of negative bleaching signal, however, varies depending on the photoexcitation wavelength (**Figure 4.5c** and **4.5d**). The change in decay rate is especially prominent for PcCu COF suggesting longer lived charge separated state. The best fit of signals yielded 3.382 ns lifetime of interlayer CT for PcCu COF and 1.228 ns for PcNi COF. These numbers are not in line with previously reported lifetimes of charge-separated states, which were shown to lie within tens of microseconds.[23,63] A major source of limitation in our work appears due to measurement of transient signals with the help of femtosecond TA spectroscopy, which limits the time window to 5 ns. In order to get evidence on the long-lived charge-separated state and their nature, we need to implement nanosecond TA spectroscopy. Besides, the decrease in the lifetime of interlayer charge transfer can be explained by poor π-stacking interaction. Lone pair from oxygen atoms

linking donor and acceptor units may prevent the formation donor-to-donor and acceptor-to-acceptor π-columns. Based on obtainable data the excited state dynamics can be summarized according to the mechanism provided in **Scheme 4.2.**

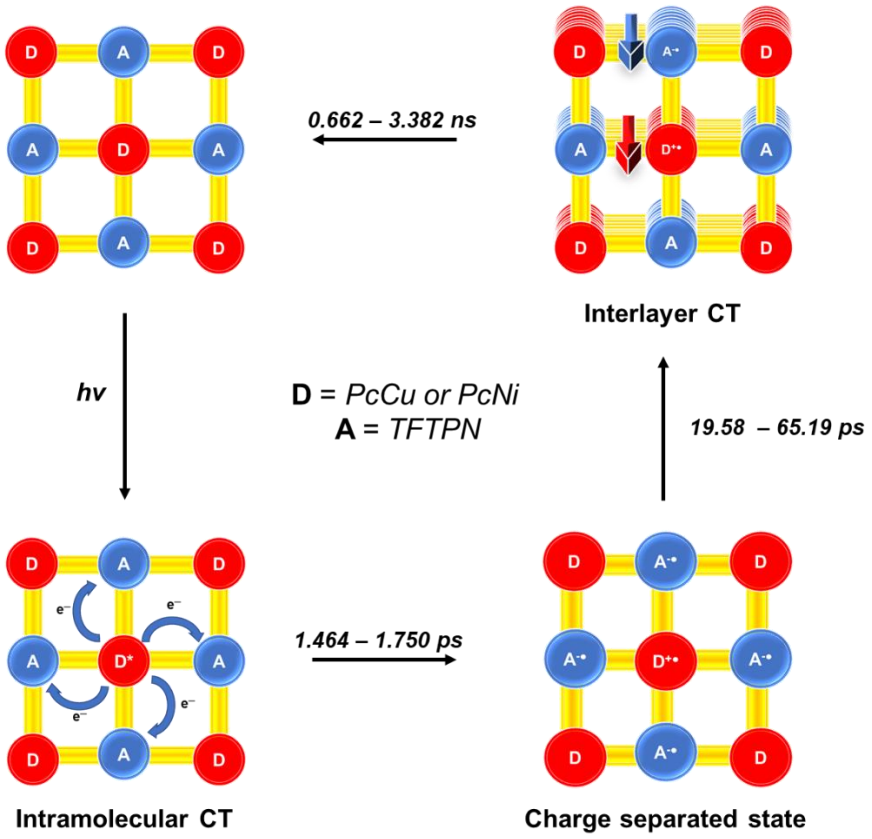

Scheme 4.2. Schematic representation of donor-acceptor interactions in metallophthalocyanine COFs

Another important finding of this study was the difference in the lifetime of charge separated state between PcCu and PcNi COFs, which are summarized in **Table 4.1** The time constant for charge recombination at 300 nm excitation is ns and ns for PcCu and PcNi COFs respectively. The results were directly compared with the previously reported findings on the lifetimes of electron migration in the columns of metallophthalocyanine COFs. Jiang *et.al.* in 2015 showed that copper phthalocyanine-naphthalene diamide COF

had realatively longer lifetime (33 us) compared to nickel version (26 - 29 us). These results agree well with our observations and can be explained by stronger ionization potential of copper phthalocyanine. Interestingly, the research of Jiang *et.al.* showed that the time constant for charge recombination is not significantly dependent on the nature of acceptor (naphthalene diimide and pyrommellitic diimide) that they incorporated into the COF. This suggests future directions of assembly metallophthalocyanine donor with acceptors varying in electron affinity.

Table 4.1. Exciton lifetimes of PcCu and PcNi COFs

Time Constant	τ_1	τ_2	τ_3
300 nm excitation			
PcCu-COF	1.750 ps	72.68 ps	3.382 ns
PcNi-COF	1.927 ps	29.15 ps	1.228 ps
650 nm excitation			
PcCu-COF	1.525 ps	65.19 ps	1.438 ns
PcNi-COF	1.464 ps	19.58 ps	0.662 ns

4.4. Conclusion.

In summary, electron transfer and charge dynamics processes were investigated for thin films of donor-acceptor metallophthalocyanine COFs using time-resolved TA spectroscopic technique. Upon photoexcitation of electron-rich metallophthalocyanine unit electron is transferred to proximate TFTPN units triggering intramolecular charge transfer process. High-order arrangement of COF layers to form π-columns can facilitate delocalization of free electron inhibiting rapid charge recombination between adjacent donor-acceptor units. The analysis of charge dynamics for metallophthalocyanine COFs builds a fundamental understanding and assists for further practical application in

photovoltaics and optoelectronics. Further adjustments in the structure of the COFs can offer promising efficient organic semiconducting material.

BIBLIOGRAPHY

(1) Berera, R.; van Grondelle, R.; Kennis, J. T. M. Ultrafast Transient Absorption Spectroscopy: Principles and Application to Photosynthetic Systems. *Photosynth. Res.* **2009**, *101* (2–3), 105–118.

(2) Westeberhard, M. J.; Smith, J. A. C.; Winter, K. Photosynthesis, Reorganized. **2011**, *332* (April).

(3) Colbow, K.; Danyluk, R. P. (1976) 107-121 Elsevier Scientific Publishing Company, Amsterdam - Printed in The Netherlands. **1976**, *440*, 107–121.

(4) Hu, Q.; Miyashita, H.; Iwasaki, I.; Kurano, N.; Miyachi, S.; Iwaki, M.; Itoh, S. A Photosystem I Reaction Center Driven by Chlorophyll d in Oxygenic Photosynthesis. *Proc. Natl. Acad. Sci. U. S. A.* **1998**, *95* (22), 13319–13323.

(5) Gur, I.; Fromer, N. a; Geier, M. L.; Alivisatos, a P. R EPORTS from Solution. *Science (80-.).* **2005**, *310* (October), 462–466.

(6) Vyas, V. S.; Haase, F.; Stegbauer, L.; Savasci, G.; Podjaski, F.; Ochsenfeld, C.; Lotsch, B. V. A Tunable Azine Covalent Organic Framework Platform for Visible Light-Induced Hydrogen Generation. *Nat. Commun.* **2015**, *6*, 1–9.

(7) Shao, L.; Li, Y.; Huang, J.; Liu, Y. N. Synthesis of Triazine-Based Porous Organic Polymers Derived N-Enriched Porous Carbons for CO2 Capture. *Ind. Eng. Chem. Res.* **2018**, *57* (8), 2856–2865.

(8) Misra, R.; Bhattacharyya, S. P. *Intramolecular Charge Transfer*; Wiley-VCH Verlag GmbH & Co. KGaA: Weinheim, Germany, 2018.

(9) Kuss-Petermann, M.; Wenger, O. S. Increasing Electron-Transfer Rates with Increasing Donor-Acceptor Distance. *Angew. Chemie - Int. Ed.* **2016**, *55* (2), 815–819.

(10) Luo, Y.; Barthelmes, K.; Wächtler, M.; Winter, A.; Schubert, U. S.; Dietzek, B. Increased Charge Separation Rates with Increasing Donor-Acceptor Distance in Molecular Triads: The Effect of Solvent Polarity. *J. Phys. Chem. C* **2017**, *121* (17), 9220–9229.

(11) Patwardhan, S.; Schatz, G. C. Theoretical Investigation of Charge Transfer in Metal Organic Frameworks for Electrochemical Device Applications. *J. Phys. Chem. C* **2015**, *119* (43), 24238–24247.

(12) Walther, M. E.; Wenger, O. S. Hole Tunneling and Hopping in a Ru(Bpy)3 2+-Phenothiazine Dyad with a Bridge Derived from Oligo-p-Phenylene. *Inorg. Chem.* **2011**, *50* (21), 10901–10907.

(13) Goldsmith, R. H.; DeLeon, O.; Wilson, T. M.; Finkelstein-Shapiro, D.; Ratner, M. A.; Wasielewski, M. R. Challenges in Distinguishing Superexchange and Hopping Mechanisms of Intramolecular Charge Transfer through Fluorene Oligomers. *J. Phys. Chem. A* **2008**, *112* (19), 4410–4414.

(14) Paulson, B. P.; Miller, J. R.; Gan, W. X.; Closs, G. Superexchange and Sequential Mechanisms in Charge Transfer with a Mediating State between the Donor and Acceptor. *J. Am. Chem. Soc.* **2005**, *127* (13), 4860–4868.

(15) Butler Ricks, A.; E. Brown, K.; Wenninger, M.; D. Karlen, S.; A. Berlin, Y.; T. Co, D.; R. Wasielewski, M. Exponential Distance Dependence of Photoinitiated Stepwise Electron Transfer in Donor–Bridge–Acceptor Molecules: Implications for Wirelike Behavior. *J. Am. Chem. Soc.* **2012**, *134* (10), 4581–4588.

(16) Wenger, O. S. How Donor - Bridge - Acceptor Energetics Influence Electron Tunneling Dynamics and Their Distance Dependences. *Acc. Chem. Res.* **2011**, *44* (1), 25–35.

(17) Dias, F. B.; Penfold, T. J.; Monkman, A. P. Photophysics of Thermally Activated Delayed Fluorescence Molecules. *Methods Appl. Fluoresc.* **2017**, *5* (1).

(18) Kim, M. J.; Yu, Y. J.; Kim, J. H.; Jung, Y. S.; Kay, K. Y.; Ko, S. B.; Lee, C. R.; Jang, I. H.; Kwon, Y. U.; Park, N. G. Tuning of Spacer Groups in Organic Dyes for Efficient Inhibition of Charge Recombination in Dye-Sensitized Solar Cells. *Dye. Pigment.* **2012**, *95* (1), 134–141.

(19) Marszalek, T.; Li, M.; Pisula, W. Design Directed Self-Assembly of Donor-Acceptor Polymers. *Chem. Commun.* **2016**, *52* (73), 10938–10947.

(20) Lei, T.; Cao, Y.; Fan, Y.; Liu, C. J.; Yuan, S. C.; Pei, J. High-Performance Air-Stable Organic Field-Effect Transistors: Isoindigo-Based Conjugated Polymers. *J. Am. Chem. Soc.* **2011**, *133* (16), 6099–6101.

(21) Mishra, A.; Ma, C. Q.; Bäuerle, P. Functional Oligothiophenes: Molecular Design for Multidimensional Nanoarchitectures and Their Applications. *Chemical Reviews*. American Chemical Society March 11, 2009, pp 1141–1176..

(22) Geng, K.; He, T.; Liu, R.; Tan, K. T.; Li, Z.; Tao, S.; Gong, Y.; Jiang, Q.; Jiang, D. Covalent Organic Frameworks: Design, Synthesis, and Functions. *Chem. Rev.* **2020**.

(23) Jin, S.; Ding, X.; Feng, X.; Supur, M.; Furukawa, K.; Takahashi, S.; Addicoat, M.; El-Khouly, M. E.; Nakamura, T.; Irle, S.; et al. Charge Dynamics in a Donor-Acceptor Covalent Organic Framework with Periodically Ordered Bicontinuous Heterojunctions. *Angew. Chemie - Int. Ed.* **2013**, *52* (7), 2017–2021.

(24) Kim, T. W.; Jun, S.; Ha, Y.; Yadav, R. K.; Kumar, A.; Yoo, C. Y.; Oh, I.; Lim, H. K.; Shin, J. W.; Ryoo, R.; et al. Ultrafast Charge Transfer Coupled with Lattice Phonons in Two-Dimensional Covalent Organic Frameworks. *Nat. Commun.* **2019**, *10* (1).

(25) Cooper, A. I. Conjugated Microporous Polymers. *Adv. Mater.* **2009**, *21* (12), 1291–1295.

(26) Feng, X.; Ding, X.; Jiang, D. Covalent Organic Frameworks. *Chem. Soc. Rev.* **2012**, *41* (18), 6010–6022.

(27) Dalapati, S.; Jin, E.; Addicoat, M.; Heine, T.; Jiang, D. Highly Emissive Covalent Organic Frameworks. *J. Am. Chem. Soc.* **2016**, *138* (18), 5797–5800.

(28) Côté, A. P.; Benin, A. I.; Ockwig, N. W.; O'Keeffe, M.; Matzger, A. J.; Yaghi, O. M. Chemistry: Porous, Crystalline, Covalent Organic Frameworks. *Science (80-.).* **2005**, *310* (5751), 1166–1170.

(29) Chen, X.; Addicoat, M.; Jin, E.; Zhai, L.; Xu, H.; Huang, N.; Guo, Z.; Liu, L.; Irle, S.; Jiang, D. Locking Covalent Organic Frameworks with Hydrogen Bonds: General and Remarkable Effects on Crystalline Structure, Physical Properties, and Photochemical Activity. *J. Am. Chem. Soc.* **2015**, *137* (9), 3241–3247.

(30) Nagai, A.; Chen, X.; Feng, X.; Ding, X.; Guo, Z.; Jiang, D. A Squaraine-Linked Mesoporous Covalent Organic Framework. *Angew. Chemie Int. Ed.* **2013**, *52* (13), 3770–3774.

(31) Vyas, V. S.; Lau, V. W. H.; Lotsch, B. V. Soft Photocatalysis: Organic Polymers for Solar Fuel Production. *Chemistry of Materials*. American Chemical Society August 9, 2016, pp 5191–5204.

(32) Banerjee, T.; Gottschling, K.; Savasci, G.; Ochsenfeld, C.; Lotsch, B. V. H2 Evolution with Covalent Organic Framework Photocatalysts. *ACS Energy Lett.* **2018**, *3* (2), 400–409.

(33) Yan, Y.; He, T.; Zhao, B.; Qi, K.; Liu, H.; Xia, B. Y. Metal/Covalent-Organic Frameworks-Based Electrocatalysts for Water Splitting. *Journal of Materials Chemistry A*. Royal Society of Chemistry August 21, 2018, pp 15905–15926.

(34) Ding, X.; Guo, J.; Feng, X.; Honsho, Y.; Guo, J.; Seki, S.; Maitarad, P.; Saeki, A.; Nagase, S.; Jiang, D. Synthesis of Metallophthalocyanine Covalent Organic Frameworks That Exhibit High Carrier Mobility and Photoconductivity. *Angew. Chemie Int. Ed.* **2011**, *50* (6), 1289–1293.

(35) Wan, S.; Guo, J.; Kim, J.; Ihee, H.; Jiang, D. A Belt-Shaped, Blue Luminescent, and Semiconducting Covalent Organic Framework. *Angew. Chemie Int. Ed.* **2008**, *47* (46), 8826–8830.

(36) Ding, X.; Chen, L.; Honsho, Y.; Feng, X.; Saengsawang, O.; Guo, J.; Saeki, A.; Seki, S.; Irle, S.; Nagase, S.; et al. An N-Channel Two-Dimensional Covalent Organic Framework. *J. Am. Chem. Soc.* **2011**, *133* (37), 14510–14513.

(37) Wan, S.; Guo, J.; Kim, J.; Ihee, H.; Jiang, D. A Photoconductive Covalent Organic Framework: Self-Condensed Arene Cubes Composed of Eclipsed 2D Polypyrene Sheets for Photocurrent Generation. *Angew. Chemie Int. Ed.* **2009**, *48* (30), 5439–5442.

(38) Rager, S.; Dogru, M.; Werner, V.; Gavryushin, A.; Götz, M.; Engelke, H.; Medina, D. D.; Knochel, P.; Bein, T. Pore Wall Fluorescence Labeling of Covalent Organic Frameworks. *CrystEngComm* **2017**, *19* (33), 4886–4891.

(39) Gao, Q.; Li, X.; Ning, G. H.; Leng, K.; Tian, B.; Liu, C.; Tang, W.; Xu, H. Sen; Loh, K. P. Highly Photoluminescent Two-Dimensional Imine-Based Covalent

Organic Frameworks for Chemical Sensing. *Chem. Commun.* **2018**, *54* (19), 2349–2352.

(40) Ma, L.; Feng, X.; Wang, S.; Wang, B. Recent Advances in AIEgen-Based Luminescent Metal-Organic Frameworks and Covalent Organic Frameworks. *Materials Chemistry Frontiers*. Royal Society of Chemistry December 1, 2017, pp 2474–2486.

(41) Crowe, J. W.; Baldwin, L. A.; McGrier, P. L. Luminescent Covalent Organic Frameworks Containing a Homogeneous and Heterogeneous Distribution of Dehydrobenzoannulene Vertex Units. *J. Am. Chem. Soc.* **2016**, *138* (32), 10120–10123.

(42) Deblase, C. R.; Hernández-Burgos, K.; Silberstein, K. E.; Rodríguez-Calero, G. G.; Bisbey, R. P.; Abruña, H. D.; Dichtel, W. R. Rapid and Efficient Redox Processes within 2D Covalent Organic Framework Thin Films. *ACS Nano* **2015**, *9* (3), 3178–3183.

(43) Zha, Z.; Xu, L.; Wang, Z.; Li, X.; Pan, Q.; Hu, P.; Lei, S. 3D Graphene Functionalized by Covalent Organic Framework Thin Film as Capacitive Electrode in Alkaline Media. *ACS Appl. Mater. Interfaces* **2015**, *7* (32), 17837–17843.

(44) Khattak, A. M.; Ghazi, Z. A.; Liang, B.; Khan, N. A.; Iqbal, A.; Li, L.; Tang, Z. A Redox-Active 2D Covalent Organic Framework with Pyridine Moieties Capable of Faradaic Energy Storage. *J. Mater. Chem. A* **2016**, *4* (42), 16312–16317.

(45) Deblase, C. R.; Silberstein, K. E.; Truong, T. T.; Abruña, H. D.; Dichtel, W. R. β-Ketoenamine-Linked Covalent Organic Frameworks Capable of Pseudocapacitive Energy Storage. *J. Am. Chem. Soc.* **2013**, *135* (45), 16821–16824.

(46) Chandra, S.; Kundu, T.; Dey, K.; Addicoat, M.; Heine, T.; Banerjee, R. Interplaying Intrinsic and Extrinsic Proton Conductivities in Covalent Organic Frameworks. *Chem. Mater.* **2016**, *28* (5), 1489–1494.

(47) Xu, H.; Tao, S.; Jiang, D. Proton Conduction in Crystalline and Porous Covalent Organic Frameworks. *Nat. Mater.* **2016**, *15* (7), 722–726.

(48) Peng, Y.; Xu, G.; Hu, Z.; Cheng, Y.; Chi, C.; Yuan, D.; Cheng, H.; Zhao, D. Mechanoassisted Synthesis of Sulfonated Covalent Organic Frameworks with High Intrinsic Proton Conductivity. *ACS Appl. Mater. Interfaces* **2016**, *8* (28), 18505–18512.

(49) Chandra, S.; Kundu, T.; Kandambeth, S.; Babarao, R.; Marathe, Y.; Kunjir, S. M.; Banerjee, R. Phosphoric Acid Loaded Azo (-N=N-) Based Covalent Organic Framework for Proton Conduction. *J. Am. Chem. Soc.* **2014**, *136* (18), 6570–6573.

(50) Lin, G.; Gao, C.; Zheng, Q.; Lei, Z.; Geng, H.; Lin, Z.; Yang, H.; Cai, Z. Room-Temperature Synthesis of Core-Shell Structured Magnetic Covalent Organic Frameworks for Efficient Enrichment of Peptides and Simultaneous Exclusion of Proteins. *Chem. Commun.* **2017**, *53* (26), 3649–3652.

(51) Wang, R.-Q.; Wei, X.-B.; Feng, Y.-Q. β-Cyclodextrin Covalent Organic Framework for Selective Molecular Adsorption. *Chem. - A Eur. J.* **2018**, *24* (43), 10979–10983.

(52) Li, Y.; Yang, C. X.; Yan, X. P. Controllable Preparation of Core-Shell Magnetic Covalent-Organic Framework Nanospheres for Efficient Adsorption and Removal of Bisphenols in Aqueous Solution. *Chem. Commun.* **2017**, *53* (16), 2511–2514.

(53) He, S.; Zeng, T.; Wang, S.; Niu, H.; Cai, Y. Facile Synthesis of Magnetic Covalent Organic Framework with Three-Dimensional Bouquet-like Structure for Enhanced Extraction of Organic Targets. *ACS Appl. Mater. Interfaces* **2017**, *9* (3), 2959–2965.

(54) Niu, X.; Ding, S.; Wang, W.; Xu, Y.; Xu, Y.; Chen, H.; Chen, X. Separation of Small Organic Molecules Using Covalent Organic Frameworks-LZU1 as Stationary Phase by Open-Tubular Capillary Electrochromatography. *J. Chromatogr. A* **2016**, *1436*, 109–117.

(55) Bao, T.; Tang, P.; Kong, D.; Mao, Z.; Chen, Z. Polydopamine-Supported Immobilization of Covalent-Organic Framework-5 in Capillary as Stationary Phase for Electrochromatographic Separation. *J. Chromatogr. A* **2016**, *1445*, 140–148.

(56) Yan, T.; Lan, Y.; Tong, M.; Zhong, C. Screening and Design of Covalent Organic Framework Membranes for CO2/CH4 Separation. *ACS Sustain. Chem. Eng.* **2019**, *7* (1), 1220–1227.

(57) Mitra, S.; Kandambeth, S.; Biswal, B. P.; Abdul Khayum, M.; Choudhury, C. K.; Mehta, M.; Kaur, G.; Banerjee, S.; Prabhune, A.; Verma, S.; et al. Self-Exfoliated Guanidinium-Based Ionic Covalent Organic Nanosheets (ICONs). *J. Am. Chem. Soc.* **2016**, *138* (8), 2823–2828.

(58) Fang, Q.; Wang, J.; Gu, S.; Kaspar, R. B.; Zhuang, Z.; Zheng, J.; Guo, H.; Qiu, S.; Yan, Y. 3D Porous Crystalline Polyimide Covalent Organic Frameworks for Drug Delivery. *J. Am. Chem. Soc.* **2015**, *137* (26), 8352–8355.

(59) Huang, N.; Zhai, L.; Coupry, D. E.; Addicoat, M. A.; Okushita, K.; Nishimura, K.; Heine, T.; Jiang, D. Multiple-Component Covalent Organic Frameworks. *Nat. Commun.* **2016**, *7* (1), 1–12.

(60) Dalapati, S.; Addicoat, M.; Jin, S.; Sakurai, T.; Gao, J.; Xu, H.; Irle, S.; Seki, S.; Jiang, D. Rational Design of Crystalline Supermicroporous Covalent Organic Frameworks with Triangular Topologies. *Nat. Commun.* **2015**, *6* (1), 1–8.

(61) Ding, S. Y.; Wang, W. Covalent Organic Frameworks (COFs): From Design to Applications. *Chemical Society Reviews*. The Royal Society of Chemistry January 21, 2013, pp 548–568.

(62) Bisbey, R. P.; Dichtel, W. R. Covalent Organic Frameworks as a Platform for Multidimensional Polymerization. *ACS Cent. Sci.* **2017**, *3* (6), 533–543.

(63) Jin, S.; Supur, M.; Addicoat, M.; Furukawa, K.; Chen, L.; Nakamura, T.;

Fukuzumi, S.; Irle, S.; Jiang, D. Creation of Superheterojunction Polymers via Direct Polycondensation: Segregated and Bicontinuous Donor-Acceptor π-Columnar Arrays in Covalent Organic Frameworks for Long-Lived Charge Separation. *J. Am. Chem. Soc.* **2015**, *137* (24), 7817–7827.

(64) Fuller, M. J.; Gusev, A. V.; Wasielewski, M. R. Ultrafast Charge Separation Due to Excited State Symmetry Breaking in Dimers of Push-Pull Perylenes. *Isr. J. Chem.* **2004**, *44* (1–3), 101–108.

(65) Luo, J.; Lu, J.; Zhang, J. Carbazole–Triazine Based Donor–Acceptor Porous Organic Frameworks for Efficient Visible-Light Photocatalytic Aerobic Oxidation Reactions. *J. Mater. Chem. A* **2018**, *6* (31), 15154–15161.

(66) Clough, A. J.; Yoo, J. W.; Mecklenburg, M. H.; Marinescu, S. C. Two-Dimensional Metal-Organic Surfaces for Efficient Hydrogen Evolution from Water. *J. Am. Chem. Soc.* **2015**, *137* (1), 118–121.

(67) Chen, X. Q.; Yao, X.; Bai, T.; Ling, J.; Xiao, W. J.; Wang, J.; Wu, S. C.; Liu, L. N.; Xie, G.; Li, J.; et al. Donor–Acceptor Photovoltaic Polymers Based on 1,4-Dithienyl-2,5-Dialkoxybenzene with Intramolecular Noncovalent Interactions. *J. Polym. Sci. Part A Polym. Chem.* **2018**, *56* (7), 689–698.

(68) Mei, C. Y.; Liang, L.; Zhao, F. G.; Wang, J. T.; Yu, L. F.; Li, Y. X.; Li, W. S. A Family of Donor-Acceptor Photovoltaic Polymers with Fused 4,7-Dithienyl-2,1,3-Benzothiadiazole Units: Effect of Structural Fusion and Side Chains. *Macromolecules* **2013**, *46* (19), 7920–7931.

(69) Chang, C. H.; Kuo, M. C.; Lin, W. C.; Chen, Y. T.; Wong, K. T.; Chou, S. H.; Mondal, E.; Kwong, R. C.; Xia, S.; Nakagawa, T.; et al. A Dicarbazole-Triazine Hybrid Bipolar Host Material for Highly Efficient Green Phosphorescent OLEDs. *J. Mater. Chem.* **2012**, *22* (9), 3832–3838.

(70) Youn Lee, S.; Yasuda, T.; Nomura, H.; Adachi, C. High-Efficiency Organic Light-Emitting Diodes Utilizing Thermally Activated Delayed Fluorescence from Triazine-Based Donor-Acceptor Hybrid Molecules. *Appl. Phys. Lett.* **2012**, *101* (9), 1–5.

(71) Yuen, J. D.; Fan, J.; Seifter, J.; Lim, B.; Hufschmid, R.; Heeger, A. J.; Wudl, F. High Performance Weak Donor-Acceptor Polymers in Thin Film Transistors: Effect of the Acceptor on Electronic Properties, Ambipolar Conductivity, Mobility, and Thermal Stability. *J. Am. Chem. Soc.* **2011**, *133* (51), 20799–20807.

(72) Ren, S.; Zeng, D.; Zhong, H.; Wang, Y.; Qian, S.; Fang, Q. Convergent Synthesis and Multifunctional Properties. *J. Phys. Chem. B* **2010**, *114*, 10374–10383.

(73) Weiss, E. A.; Ahrens, M. J.; Sinks, L. E.; Ratner, M. A.; Wasielewski, M. R. Solvent Control of Spin-Dependent Charge Recombination Mechanisms within Donor-Conjugated Bridge-Acceptor Molecules. *J. Am. Chem. Soc.* **2004**, *126* (31), 9510–9511.

(74) Ricks, A. B.; Solomon, G. C.; Colvin, M. T.; Scott, A. M.; Chen, K.; Ratner, M.

A.; Wasielewski, M. R. Controlling Electron Transfer in Donor-Bridge-Acceptor Molecules Using Cross-Conjugated Bridges. *J. Am. Chem. Soc.* **2010**, *132* (43), 15427–15434.

(75) Zhao, L.; Liu, C. F.; Xu, W. D.; Jiang, Y.; Lai, W. Y.; Huang, W. Donor-Acceptor Star-Shaped Conjugated Macroelectrolytes: Synthesis, Light-Harvesting Properties, and Self-Assembly-Induced Förster Resonance Energy Transfer. *J. Phys. Chem. B* **2015**, *119* (22), 6730–6739.

(76) Ponomarenko, S. A.; Luponosov, Y. N.; Min, J.; Solodukhin, A. N.; Surin, N. M.; Shcherbina, M. A.; Chvalun, S. N.; Ameri, T.; Brabec, C. Design of Donor-Acceptor Star-Shaped Oligomers for Efficient Solution-Processible Organic Photovoltaics. *Faraday Discuss.* **2014**, *174*, 313–339.

(77) Bakirov, A. V.; Solodukhin, A. N.; Luponosov, Y. N.; Svidchenko, E. A.; Obrezkova, M. A.; Peregudova, S. M.; Shcherbina, M. A.; Ponomarenko, S. A.; Chvalun, S. N. The Effect of Star-Shaped Oligothiophenes with a Carbazole Core on Their Structural and Optical Properties. *Nanotechnologies Russ.* **2017**, *12* (7–8), 385–394.

(78) Sun, Z.; Jiang, Y.; Zeng, L.; Huang, L. Intramolecular Charge Transfer and Extended Conjugate Effects in Donor–Π–Acceptor-Type Mesoporous Carbon Nitride for Photocatalytic Hydrogen Evolution. *ChemSusChem* **2019**, *12* (7), 1325–1333.

(79) Pan, J. Y.; Zuo, L. J.; Hu, X. L.; Fu, W. F.; Chen, M. R.; Fu, L.; Gu, X.; Shi, H. Q.; Shi, M. M.; Li, H. Y.; et al. Star-Shaped D-A Small Molecules Based on Diketopyrrolopyrrole and Triphenylamine for Efficient Solution-Processed Organic Solar Cells. *ACS Appl. Mater. Interfaces* **2013**, *5* (3), 972–980.

(80) Wu, H. C.; Zhang, J.; Bo, Z.; Chen, W. C. Well-Defined Star-Shaped Donor-Acceptor Conjugated Molecules for Organic Resistive Memory Devices. *Chem. Commun.* **2015**, *51* (75), 14179–14182.

(81) Davis, W. B.; Ratner, M. A.; Wasielewski, M. R. Conformational Gating of Long Distance Electron Transfer through Wire-like Bridges in Donor−Bridge−Acceptor Molecules. *J. Am. Chem. Soc.* **2001**, *123* (32), 7877–7886.

(82) Albinsson, B.; Eng, M. P.; Pettersson, K.; Winters, M. U. Electron and Energy Transfer in Donor–Acceptor Systems with Conjugated Molecular Bridges. *Phys. Chem. Chem. Phys.* **2007**, *9* (44), 5847–5864.

(83) Daub, J.; Engl, R.; Kurzawa, J.; Miller, S. E.; Schneider, S.; Stockmann, A.; Wasielewski, M. R. Competition between Conformational Relaxation and Intramolecular Electron Transfer within Phenothiazine−Pyrene Dyads. *J. Phys. Chem. A* **2001**, *105* (23), 5655–5665.

(84) Seok Oh, C.; de Sa Pereira, D.; Hyun Han, S.; Park, H.-J.; F. Higginbotham, H.; P. Monkman, A.; Yeob Lee, J. Dihedral Angle Control of Blue Thermally Activated Delayed Fluorescent Emitters through Donor Substitution Position for Efficient Reverse Intersystem Crossing. *ACS Appl. Mater. & Interfaces* **2018**, *10* (41),

(85) Buck, J. T.; Boudreau, A. M.; DeCarmine, A.; Wilson, R. W.; Hampsey, J.; Mani, T. Spin-Allowed Transitions Control the Formation of Triplet Excited States in Orthogonal Donor-Acceptor Dyads. *Chem* **2019**, *5* (1), 138–155.

(86) Piontkowski, Z.; W. McCamant, D. Excited-State Planarization in Donor–Bridge Dye Sensitizers: Phenylene versus Thiophene Bridges. *J. Am. Chem. Soc.* **2018**, *140* (35), 11046–11057.

(87) Liang, X.; Zhang, Q. Recent Progress on Intramolecular Charge-Transfer Compounds as Photoelectric Active Materials. *Sci. China Mater.* **2017**, *60* (11), 1093–1101.

(88) Davis, M. E. New Vistas in Zeolite and Molecular Sieve Catalysis. *Acc. Chem. Res.* **1993**, *26* (3), 111–115.

(89) Xiao, P.; Zhao, Y.; Wang, T.; Zhan, Y.; Wang, H.; Li, J.; Thomas, A.; Zhu, J. Polymeric Carbon Nitride/Mesoporous Silica Composites as Catalyst Support for Au and Pt Nanoparticles. *Chem. - A Eur. J.* **2014**, *20* (10), 2872–2878.

(90) Pereira, M. F. R.; Orfão, J. J. M.; Figueiredo, J. L. Oxidative Dehydrogenation of Ethylbenzene on Activated Carbon Catalysts 2. Kinetic Modelling. *Appl. Catal. A Gen.* **2000**, *196* (1), 43–54.

(91) Kaur, P.; Hupp, J. T.; Nguyen, S. T. Porous Organic Polymers in Catalysis: Opportunities and Challenges. *ACS Catal.* **2011**, *1* (7), 819–835.

(92) Thommes, M.; Kaneko, K.; Neimark, A. V.; Olivier, J. P.; Rodriguez-Reinoso, F.; Rouquerol, J.; Sing, K. S. W. Physisorption of Gases, with Special Reference to the Evaluation of Surface Area and Pore Size Distribution (IUPAC Technical Report). *Pure Appl. Chem.* **2015**, *87* (9–10), 1051–1069.

(93) Férey, G. Hybrid Porous Solids: Past, Present, Future. *Chem. Soc. Rev.* **2008**, *37* (1), 191–214.

(94) Lee, Y. R.; Kim, J.; Ahn, W. S. Synthesis of Metal-Organic Frameworks: A Mini Review. *Korean J. Chem. Eng.* **2013**, *30* (9), 1667–1680.

(95) Evans, A. M.; Parent, L. R.; Flanders, N. C.; Busbey, R. P.; Vitaku, E.; Kirschner, M. S.; Schaller, R. D.; Chen, L. X.; Gianneschi, N. C.; Dichtel, W. R. Organic Frameworks. *Science (80-.).* **2018**, *361* (July), 52–57.

(96) Byun, Y.; Je, S. H.; Talapaneni, S. N.; Coskun, A. Advances in Porous Organic Polymers for Efficient Water Capture. *Chem. - A Eur. J.* **2019**, *25* (44), 10262–10283.

(97) Zhang, X.; Lu, J.; Zhang, J. Porosity Enhancement of Carbazolic Porous Organic Frameworks Using Dendritic Building Blocks for Gas Storage and Separation. *Chem. Mater.* **2014**, *26* (13), 4023–4029.

(98) Ding, X.; Li, H.; Zhao, Y. C.; Han, B. H. Mannitol-Based Acetal-Linked Porous Organic Polymers for Selective Capture of Carbon Dioxide over Methane. *Polym. Chem.* **2015**, *6* (29), 5305–5312.

(99) Wood, C. D.; Tan, B.; Trewin, A.; Su, F.; Rosseinsky, M. J.; Bradshaw, D.; Sun, Y.; Zhou, L.; Cooper, A. I. Microporous Organic Polymers for Methane Storage. *Adv. Mater.* **2008**, *20* (10), 1916–1921.

(100) Yuan, S.; Dorney, B.; White, D.; Kirklin, S.; Zapol, P.; Yu, L.; Liu, D. J. Microporous Polyphenylenes with Tunable Pore Size for Hydrogen Storage. *Chem. Commun.* **2010**, *46* (25), 4547–4549.

(101) Rao, K. V.; Mohapatra, S.; Maji, T. K.; George, S. J. Guest-Responsive Reversible Swelling and Enhanced Fluorescence in a Super-Absorbent, Dynamic Microporous Polymer. *Chem. - A Eur. J.* **2012**, *18* (15), 4505–4509.

(102) Wang, X. Sen; Liu, J.; Bonefont, J. M.; Yuan, D. Q.; Thallapally, P. K.; Ma, S. A Porous Covalent Porphyrin Framework with Exceptional Uptake Capacity of Saturated Hydrocarbons for Oil Spill Cleanup. *Chem. Commun.* **2013**, *49* (15), 1533–1535.

(103) Wang, Z. J.; Ghasimi, S.; Landfester, K.; Zhang, K. A. I. Highly Porous Conjugated Polymers for Selective Oxidation of Organic Sulfides under Visible Light. *Chem. Commun.* **2014**, *50* (60), 8177–8180.

(104) Kang, N.; Park, J. H.; Ko, K. C.; Chun, J.; Kim, E.; Shin, H. W.; Lee, S. M.; Kim, H. J.; Ahn, T. K.; Lee, J. Y.; et al. Tandem Synthesis of Photoactive Benzodifuran Moieties in the Formation of Microporous Organic Networks. *Angew. Chemie - Int. Ed.* **2013**, *52* (24), 6228–6232.

(105) Xu, C.; Zhang, W.; Tang, J.; Pan, C.; Yu, G. Porous Organic Polymers: An Emerged Platform for Photocatalytic Water Splitting. *Front. Chem.* **2018**, *6* (DEC).

(106) Patwardhan, S.; Kocherzhenko, A. A.; Grozema, F. C.; Siebbeles, L. D. A. Delocalization and Mobility of Charge Carriers in Covalent Organic Frameworks. *J. Phys. Chem. C* **2011**, *115* (23), 11768–11772.

(107) Koo, B. T.; Berard, P. G.; Clancy, P. A Kinetic Monte Carlo Study of Fullerene Adsorption within a Pc-PBBA Covalent Organic Framework and Implications for Electron Transport. *J. Chem. Theory Comput.* **2015**, *11* (3), 1172–1180.

(108) Calik, M.; Auras, F.; Salonen, L. M.; Bader, K.; Grill, I.; Handloser, M.; Medina, D. D.; Dogru, M.; Löbermann, F.; Trauner, D.; et al. Extraction of Photogenerated Electrons and Holes from a Covalent Organic Framework Integrated Heterojunction. *J. Am. Chem. Soc.* **2014**, *136* (51), 17802–17807.

(109) Yang, H.; Zhang, S.; Han, L.; Zhang, Z.; Xue, Z.; Gao, J.; Li, Y.; Huang, C.; Yi, Y.; Liu, H.; et al. High Conductive Two-Dimensional Covalent Organic Framework for Lithium Storage with Large Capacity. *ACS Appl. Mater. Interfaces* **2016**, *8* (8), 5366–5375.

(110) Zhao, H.; Jin, Z.; Su, H.; Jing, X.; Sun, F.; Zhu, G. Targeted Synthesis of a 2D Ordered Porous Organic Framework for Drug Release. *Chem. Commun.* **2011**, *47* (22), 6389–6391.

(111) Ma, J.; Wang, M.; Du, Z.; Chen, C.; Gao, J.; Xu, J. Synthesis and Properties of Furan-Based Imine-Linked Porous Organic Frameworks. *Polym. Chem.* **2012**, *3* (9), 2346–2349.

(112) Zou, X.; Ren, H.; Zhu, G. Topology-Directed Design of Porous Organic Frameworks and Their Advanced Applications. *Chem. Commun.* **2013**, *49* (38), 3925–3936.

(113) Hasell, T.; Chong, S. Y.; Jelfs, K. E.; Adams, D. J.; Cooper, A. I. Porous Organic Cage Nanocrystals by Solution Mixing. *J. Am. Chem. Soc.* **2012**, *134* (1), 588–598.

(114) Tautz, R.; Da Como, E.; Limmer, T.; Feldmann, J.; Egelhaaf, H. J.; Von Hauff, E.; Lemaur, V.; Beljonne, D.; Yilmaz, S.; Dumsch, I.; et al. Structural Correlations in the Generation of Polaron Pairs in Low-Bandgap Polymers for Photovoltaics. *Nat. Commun.* **2012**, *3*.

(115) Rolczynski, B. S.; Szarko, J. M.; Son, H. J.; Liang, Y.; Yu, L.; Chen, L. X. Ultrafast Intramolecular Exciton Splitting Dynamics in Isolated Low-Band-Gap Polymers and Their Implications in Photovoltaic Materials Design. *J. Am. Chem. Soc.* **2012**, *134* (9), 4142–4152.

(116) Spitler, E. L.; Dichtel, W. R. Lewis Acid-Catalysed Formation of Two-Dimensional Phthalocyanine Covalent Organic Frameworks. *Nat. Chem.* **2010**, *2* (8), 672–677.

(117) Lloyd, M. T.; Anthony, J. E.; Malliaras, G. G. Photovoltaics from Soluble Small Molecules. *Materials Today*. Elsevier November 1, 2007, pp 34–41.

(118) Feng, X.; Ding, X.; Jiang, D. Covalent Organic Frameworks. *Chemical Society Reviews*. Royal Society of Chemistry September 21, 2012, pp 6010–6022.

(119) Nagai, A.; Guo, Z.; Feng, X.; Jin, S.; Chen, X.; Ding, X.; Jiang, D. Pore Surface Engineering in Covalent Organic Frameworks. *Nat. Commun.* **2011**, *2* (1), 536.

(120) Wan, S.; Guo, J.; Kim, J.; Ihee, H.; Jiang, D. A Belt-Shaped, Blue Luminescent, and Semiconducting Covalent Organic Framework. *Angew. Chemie - Int. Ed.* **2008**, *47* (46), 8826–8830.

(121) Ding, X.; Guo, J.; Feng, X.; Honsho, Y.; Guo, J.; Seki, S.; Maitarad, P.; Saeki, A.; Nagase, S.; Jiang, D. Synthesis of Metallophthalocyanine Covalent Organic Frameworks That Exhibit High Carrier Mobility and Photoconductivity. *Angew. Chemie Int. Ed.* **2011**, *50* (6), 1289–1293.

(122) Feng, X.; Dong, Y.; Jiang, D. Star-Shaped Two-Dimensional Covalent Organic Frameworks. *CrystEngComm* **2013**, *15* (8), 1508–1511.

(123) Feng, X.; Chen, L.; Dong, Y.; Jiang, D. Porphyrin-Based Two-Dimensional Covalent Organic Frameworks: Synchronized Synthetic Control of Macroscopic Structures and Pore Parameters. *Chem. Commun.* **2011**, *47* (7), 1979–1981.

(124) Feng, X.; Liu, L.; Honsho, Y.; Saeki, A.; Seki, S.; Irle, S.; Dong, Y.; Nagai, A.; Jiang, D. High-Rate Charge-Carrier Transport in Porphyrin Covalent Organic

Frameworks: Switching from Hole to Electron to Ambipolar Conduction. *Angew. Chemie Int. Ed.* **2012**, *51* (11), 2618–2622.

(125) Feng, X.; Chen, L.; Honsho, Y.; Saengsawang, O.; Liu, L.; Wang, L.; Saeki, A.; Irle, S.; Seki, S.; Dong, Y.; et al. An Ambipolar Conducting Covalent Organic Framework with Self-Sorted and Periodic Electron Donor-Acceptor Ordering. *Adv. Mater.* **2012**, *24* (22), 3026–3031.

(126) Chen, X.; Addicoat, M.; Irle, S.; Nagai, A.; Jiang, D. Control of Crystallinity and Porosity of Covalent Organic Frameworks by Managing Interlayer Interactions Based on Self-Complementary π-Electronic Force. *J. Am. Chem. Soc.* **2013**, *135* (2), 546–549.

(127) Tang, C. W. Two-Layer Organic Photovoltaic Cell. *Appl. Phys. Lett.* **1986**, *48* (2), 183–185.

(128) Peumans, P.; Forrest, S. R. Very-High-Efficiency Double-Heterostructure Copper Phthalocyanine/C60 Photovoltaic Cells. *Appl. Phys. Lett.* **2001**, *79* (1), 126–128.

(129) Sullivan, P.; Jones, T. S.; Ferguson, A. J.; Heutz, S. Structural Templating as a Route to Improved Photovoltaic Performance in Copper Phthalocyanine/Fullerene (C60) Heterojunctions. *Appl. Phys. Lett.* **2007**, *91* (23), 233114.

(130) Ng, T. W.; Lo, M. F.; Zhou, Y. C.; Liu, Z. T.; Lee, C. S.; Kwon, O.; Lee, S. T. Ambient Effects on Fullerene/Copper Phthalocyanine Photovoltaic Interface. *Appl. Phys. Lett.* **2009**, *94* (19), 193304.

(131) Kushto, G. P.; Mäkinen, A. J.; Lane, P. A. Organic Photovoltaic Cells Using Group 10 Metallophthalocyanine Electron Donors. *IEEE J. Sel. Top. Quantum Electron.* **2010**, *16* (6), 1552–1559.

(132) Touka, N.; Benelmadjat, H.; Boudine, B.; Halimi, O.; Sebais, M. Copper Phthalocyanine Nanocrystals Embedded into Polymer Host: Preparation and Structural Characterization. *Journal of the Association of Arab Universities for Basic and Applied Sciences*. University of Bahrain 2013, pp 52–56.

(133) Farag, A. A. M. Optical Absorption Studies of Copper Phthalocyanine Thin Films. *Opt. Laser Technol.* **2007**, *39* (4), 728–732.

(134) Caplins, B. W.; Mullenbach, T. K.; Holmes, R. J.; Blank, D. A. Femtosecond to Nanosecond Excited State Dynamics of Vapor Deposited Copper Phthalocyanine Thin Films. *Phys. Chem. Chem. Phys.* **2016**, *18* (16), 11454–11459.

(135) El-Nahass, M. M.; Abd-El-Rahman, K. F.; Darwish, A. A. A. Fourier-Transform Infrared and UV-Vis Spectroscopes of Nickel Phthalocyanine Thin Films. *Mater. Chem. Phys.* **2005**, *92* (1), 185–189.

(136) Cornil, J. Influence of Interchain Interactions in the Absorption and Luminescence of Conjugated Oligomers and Polymers: A Quantum-Chemical Characterization. *J. Am. Chem. Soc.* **1998**, *120* (6), 1289–1299.

(137) Huang, T. H.; Sharp, J. H. Electronic Transitions of Vanadyl Phthalocyanine in

Solution and in the Solid State. *Chem. Phys.* **1982**, *65* (2), 205–216.

(138) Hosokawa, Y.; Yashiro, M.; Asahi, T.; Fukumura, H.; Masuhara, H. Femtosecond Laser Ablation Dynamics of Amorphous Film of a Substituted Cu-Phthalocyanine. *Appl. Surf. Sci.* **2000**, *154*, 192–195.

(139) Abramczyk, H.; Brozek-Płuska, B.; Kurczewski, K.; Kurczewska, M.; Szymczyk, I.; Krzyczmonik, P.; Błaszczyk, T.; Scholl, H.; Czajkowski, W. Femtosecond Transient Absorption, Raman, and Electrochemistry Studies of Tetrasulfonated Copper Phthalocyanine in Water Solutions. *J. Phys. Chem. A* **2006**, *110* (28), 8627–8636.